An Elementary Introduction to Atomic Force Microscopy and Related Methods

U. Hartmann

Institute of Experimental Physics, University of Saarbrücken

D-66041 Saarbrücken, Germany

Contents

Page

1.	**Introduction**	1
2.	**Scanning Probe Technology: Basic Fundamentals**	**2**
3.	**Scanning Force Microscopy**	**7**
3.1	**Force Sensors**	**7**
3.2	**State-of-the-Art Set-Ups**	**14**
3.3	**Probe-Sample Interactions**	**17**
3.4	**Contact-Mode Operation**	**20**
3.5	**Lateral Forces**	**24**
3.6	**Noncontact-Mode Operation**	**27**
3.7	**Shear-Force Microscopy**	**39**
3.8	**Force Curves and Spectroscopy**	**41**
4.	**Nanometer-Scale Modification of Surfaces**	**45**
5.	**Conlusions and Outlook**	**49**
References		**51**

Preface

The invention of a physical method which is of importance for many areas of application is usually accompanied by a huge output of dedicated publications. This is a natural process since every little step towards a progress in the particular field is reported to the community of experts being active in that respective field. With the continuously proceeding, understanding and improvement of the new method and with the availability of commercial realizations more and more researchers who have not directly been involved in the development of the new technique, but who consider it potentially relevant for their particular application contribute to a broad establishment of the invention in science and technology. Scanning probe methods have revolutionized many areas of fundamental and applied research precisely according to this scheme.

Scanning force microscopy as the most widely used variant of the scanning probe methods exhibited a strikingly successful evolution over the past ten years. Today force microscopy and related methods are used in experimental physics, in chemistry, in materials science and in biology. While the basic modes of operation are well-established and are available as commercial solutions, some highly dedicated modes of operation are permanently under development. Thus, the situation is that the number of publications dealing with force microscopy and its applications in various research areas is still considerably growing. In such a situation it is certainly very helpful, even for the expert in the field, to consult from time to time adequate overviews presenting the actual state of the art.

The present overview is by far not exhaustive. It may be helpful for the operator of a scanning probe microscope who is interested in getting some information on inner parts of the black box which he is hopefully successfully employing for his research. The article may also be helpful for those colleagues who entered the field of scanning probe methods in order to concentrate their efforts on the understanding of still not well-understood probe-sample interactions taking place upon operating scanning probe instruments and on the improvement of the methods. Finally, even the real expert may not waste time in reading the article because it provides him at least with historically important references and with key references as a link to more dedicated highly sophisticated publications. Thus, the choice of papers cited in the

following should be considered as an attempt to mention the most important preliminary approaches on the one hand and to provide links to at least some of the many interesting and striking applications on the other hand.

Saarbrücken, July 1997

U. Hartmann

1. Introduction

It is certainly not necessary to emphasize the enormous importance of microscopic imaging in the natural sciences, in medicine, and in various engineering disciplines. In the past decades this importance has been recognized repeatedly by the awarding of Nobel prices to the inventors of a number of new and improved approaches in the field of microscopy. Today a strong driving force for further developments results from the increasing demand related to key technologies. One of the key technologies is certainly microelectronics where, as a consequence of the decreasing scale of many devices, high-resolution characterization methods have become of fundamental importance for further development in this area. Another discipline, where progress is directly related to the availability of powerful microscopy methods, is certainly the development of new and functional materials. The latter strongly relies on the characterization of materials at various and increasing levels of resolution. Structure, microstructure, and defect geometry, as well as chemical composition and spatial distribution are important parameters determining the behavior of materials and practical applications.

In order to qualify a certain approach as *microscopy*, the method should give spatially localized information on the microstructure and it should have the potential to provide a magnified real-space image of the sample (Amelincks et al., 1997). A today's materials scientist, e. g., has a large number of such methods at his disposal. This is necessary because complete characterization of the given material requires the application of different and complementary characterization methods, then yielding in combination the numerous relevant parameters.

In 1980/81 G. Binnig, H. Rohrer, and coworkers from the IBM Zürich Research Laboratories invented a new type of microscope (Binnig et al., 1982) which they called the Scanning Tunneling Microscope (STM). The instrument, which proved capable of imaging solid surfaces with atomic resolution, has revolutionized microscopy and surface analysis in an unprecedented way over the past 15 years. When looking back it is evident that the outstanding success of STM is not only due to the ultrahigh resolution which can be achieved by this technique. Equally important, if not more, is that STM stimulated the development of a whole family of Scanning Probe Methods (SPM) which are all based on instrumental principles very similar to that of the STM. The most popular offsprings are Atomic Force Microscopy (AFM)

(Binnig et al., 1986), and Scanning Near-Field Optical Microscopy (SNOM) (Pohl et al., 1984). STM, AFM, and SNOM today represent a set of microscopies which can be applied in many different and highly dedicated modes of operation, such that a variety of physical and chemical properties of a material becomes accessible. This versatility of SPM in general is, apart from the inherent high resolution, a major strength. Today no materials scientist can master more than a few of all the microscopy methods based on static electric and magnetic fields, particle beams, electromagnetic radiation, acoustic waves, etc., and presumably would not have access to the instrumentation necessary to apply a number of them. On the other hand the operational principle of SPM is uniform and often a variety of physical properties can be obtained even by employing only one general-purpose set-up.

The literature in the field is vast. Among others comprehensive introductions have been given by D. A. Bonnell (1992), R. Wiesendanger and H.-J. Güntherodt (1992/93), C. J. Chen (1993), O. Marti and M. Amrein (1993), R. Wiesendanger (1994), S. N. Maganov and M.-H. Whangbo (1996), and Ch. Bai (1995). More specific information is found in the various proceedings of the international conferences on scanning tunneling microscopy and related methods (STM). The scope of this contribution is to give a brief introduction to SPM in general and to AFM and its applications in materials science in particular.

2. Scanning Probe Technology: Basic Fundamentals

Two important aspects are essential to all scanning probe methods: scanning and operating the scanned probe in near-field. While scanning is well-established in microscopy since quite some time, e. g., in electron microscopy, consequent near-field operation is a relatively novel approach in microscopy. It implies that the scanned probe has to be operated sufficiently close to the imaged sample surface.

Furthermore it is conceptually important to consider scanning probe microscopy not simply as a method where a local probe precisely maps the topography or morphology of a surface with high resolution, but as a method where the probe is used to carry out a local experiment at any position met during raster-scanning the sample surface. The results of all the successively performed experiments are collected and imaged as a function of the probe's lateral position, re-

spectively. This then yields an image of the scanned surface area from the viewpoint of the particularly chosen experimental parameters. Consequently, different operational parameters will generally result in completely different information on the scanned sample surface.

If a sharp probe, e. g., the tip terminating an extended solid probe, is in very close proximity to a sample surface, a variety of interactions can result. If the probe is at a distance of a few nanometers, van der Waals forces between probe and sample will occur. If additionally an electrical potential difference is externally applied, electrostatic interactions occur. If probe and sample are ferromagnetic, magnetostatic forces will result. If the probe-sample distance is decreased to less than about 1 nm, the application of a small potential difference leads to a local tunneling current between probe and sample, if both of them are either conducting or semiconducting. This is utilized in STM. If the proximal probe is capable of emitting or collecting light at a sub-wavelength scale, the sample surface can be imaged below the diffraction limit. This is utilized in SNOM. Suitable probes can also be operated in direct mechanical contact with the sample surface, then providing information on the surface topography, on tribological properties, as well as on the elastic and or inelastic response of the sample. Further probe-sample interactions involve near-field acoustics, thermal and ionic transfer. Apart from the detailed configuration of probe and sample and from the applied external parameters, the respective probe-sample interaction is also influenced by environmental conditions which can involve liquids as well as gases.

Near-field operation is the prerequisite for obtaining high spatial resolution by breaking diffraction limits. However, in order to experimentally utilize the potential for high resolution the probe has to be permanently kept in the near-field regime with respect to its vertical position, and lateral positioning has to be sufficiently precise. Atomic and even sub-atomic accuracy in positioning is obtained if piezoelectric actuators are employed. Utilizing the inverse piezoelectric effect a driving voltage applied to the electrodes of the actuator can be converted directly into elongations and contractions. With a suitable arrangement of piezoelectric bars forming a tripod a fully three-dimensional positioning can be achieved (Binnig and Rohrer, 1982). Along each axis the resulting length change upon applying a voltage V is

$$\Delta l = d_{31} \frac{l}{h} V \, , \tag{1}$$

where d_{31} is the piezoelectric coefficient and l and h are the length and the thickness of the bar. An even more efficient conversion of driving voltage into deflection is obtained with piezoelectric bimorphs clamped at both ends (Pohl 1986). The bimorph consists of a sandwich structure of two piezos with an inner electrode at the interface. For such a device the deflection at the center between the clamped ends is

$$\Delta h = \frac{3}{8}\, d_{31} \left(\frac{l}{h}\right)^2 V. \tag{2}$$

A very elegant way to achieve three-dimensional positioning is realized by using a piezoelectric tube of length l, wall thickness h, and inner diameter d (Binnig and Smith, 1986). The outer electrode is devided into four segments. If a voltage is applied between the inner and all outer electrodes, the length change of the tube is given by

$$\Delta l = d_{31} \frac{l}{h} V\,, \tag{3}$$

which exactly corresponds to the result in Eq. (1). However, since the wall thickness of the tube is usually much smaller than the thickness of the piezoelectric bar, the tube is much more sensitive. Upon applying two voltages of equal magnitude but opposite sign to two opposite pairs of the outer electrodes with respect to the inner electrode, deflections of the tube oriented perpendicular to its axis of symmetry can be obtained (Chen, 1992):

$$\Delta(x, y) = 2\sqrt{2}\, d_{31} \frac{l^2}{\pi d h} V_{x,y}\,. \tag{4}$$

The ability to precisely position a probe does not yet allow the stable operation of a near-field microscope. As already emphasized, it is essential that the probe is always kept in the near-field regime of the respective interaction between probe and sample (Fig. 1).

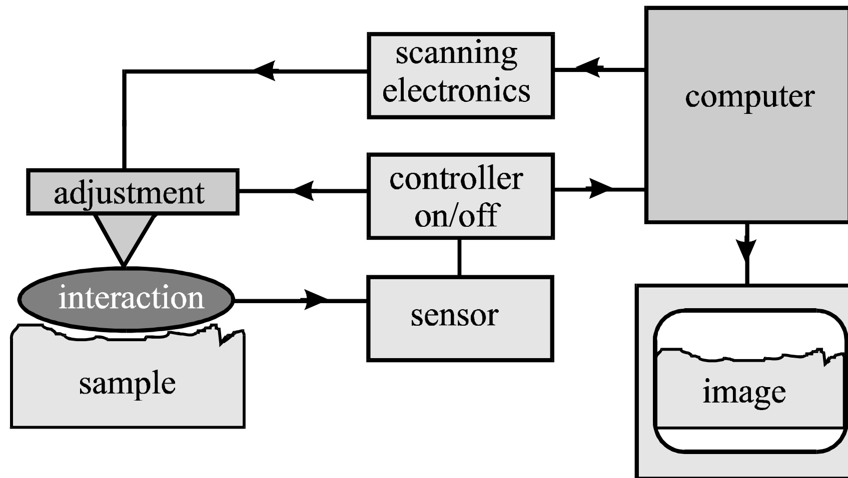

Fig. 1: *Components of a scanning probe instrument.*

In STM the interaction manifests itself in a tunneling current which depends so sensitively upon the probe-sample distance that a distance change by one atomic diameter results in a current change of one order of magnitude. It is thus essential to control in any near-field approach the probe-sample spacing by a feedback mechanism which ensures that the actually resulting interaction always corresponds to a preset value. A suitable mode of operation is then given by scanning the probe along the x and y directions upon continuously varying the vertical coordinate (z direction) such that the interaction is kept constant. This is called the *constant-interaction mode* of operation. Displaying the z driving voltage of the piezoelectric actuator as a function of the (x, y) coordinates yields a map of the local interaction all over the scanned area. The feedback-loop system usually has a PI characteristics and is realized by analog or digital set-ups. The whole system is controlled by a computer which creates the ramp signals for scanning and which serves for data acquisition, data analysis, data processing, and data visualization. The computer is linked to the microscope and to the peripheral electronics by DACs and ADCs. The peripheral electronics contains, apart from the feedback loop, suitable devices to measure the probe-sample interaction as well as the high-voltage amplifiers for driving the piezoelectric actuators.

In advanced systems the computer control also allows to employ numerous operational modes which deviate from constant-interaction scanning. These modes involve scanning at a constant average probe-sample distance, local spectroscopy, the performance of local surface modifications by increasing the probe-sample interaction, and a variety of other features which will be partly discussed below in the context of AFM.

Frequently, the task to be performed by SPM consists in scanning an arbitrary area of the sample upon detecting a particular probe-sample interaction. On the other hand, in many applications it is important to analyze a precisely given particular area of a sample, i. e., individual objects on an extended sample surface. The maximum scan range in SPM is usually between 10 µm and 100 µm. The vertical positioning of the probe achieved by the scanner is typically a few micrometers. It is thus evident that a full three-dimensional positioning of the probe with respect to the sample at a millimeter length scale is convenient. The minimum requirement is, however, that the probe-sample approach has to be performed over a few millimeters in vertical direction after inserting the sample into the microscope. The steps in forward motion involved in this vertical approach have to be smaller than the total range of the z piezodrive to avoid accidental contact between probe and sample during the approach. Furthermore, it is convenient, that the two-dimensional positioning of the probe with respect to the sample within the surface plane equally involves steps which are below the maximum scan range in order to address a particular position on the sample surface. Numerous different coarse positioning devices have been developed over the past 15 years. These involve mechanical constructions on the basis of micrometer screws and reduction levers (Demuth et al., 1986; Coombs and Pethica, 1986; Kaiser and Jaklevic, 1988) or on the basis of spring systems (Smith and Binnig, 1986; Fein et al., 1987; Wiesendanger et al., 1990 a), piezoelectric walkers (Binnig and Rohrer, 1982; Mamin et al., 1985; Uozumi et al., 1988; Takta et al., 1989), magnetic walkers (Smith and Elrod, 1985; Corb et al., 1985; Ringger et al., 1986; Wiesendanger et al., 1990 a, b), inertial sliders (Pohl, 1987; Anders et al., 1987; Niedermann et al., 1988; Lyding et al. 1988; Frohn et al., 1989), and also standard electromagnetic stepper motors which are applied in many commercial instruments today.

The design of the microscope head has to account for numerous sources of imperfections. An instrument which should yield atomic precision is sensitive to external vibrations. This sensitivity can be largely overcome by ensuring high resonant frequencies of the whole device. A sufficiently high resonant frequency and a sufficiently fast feedback system allow a high scan speed. In state-of-the-art instruments, video scan rates can be realized which is useful for studying dynamic processes. Furthermore, thermal drifts should be as low as possible. Thermal drifts result from differences in the thermal expansion coefficients of different materials and from mechanical constructions of low symmetry. They can greatly be reduced if materials with similar thermal expansion coefficients are used in conjunction with highly symmetrical

designs. Nonlinearities, hysteresis, and creep of the piezoelectric actuators can be eliminated by realtime-feedback scan correction or postimaging software corrections. In any case the piezoelectric elements have to be carefully calibrated. Cross-talk between adjacent piezoelectrodes and between the driving voltage and measured signals has to be avoided as far as possible.

A large variety of different home-built instruments has been presented by numerous groups. Additionally a couple of commercial instruments is available for STM, AFM, and SNOM, involving variants which can be operated in liquids, in ultrahigh vacuum (UHV), at low and elevated temperatures, and in high magnetic fields. From all SPM methods AFM is certainly the most versatile one which will become evident from the following discussion.

3. Scanning Force Microscopy

The most fundamental interaction between probe and sample in SPM results in forces. Forces are ever-present between two solids in close proximity and their manifestation does not require any external manipulation. In order to measure forces at a certain spatial resolution the scanning probe instrument has to be equipped with a suitable force sensor. This then leads to an instrument which has even proven capable of imaging atomic structures. It was originally called the Atomic Force Microscope (AFM) (Binnig et al., 1986), and this denotation is still widely used. However, subsequently it turned out that a force microscope can be used to analyze a variety of forces involving short- as well as long-range interactions. Since the resulting applications are much broader than only the analysis of interatomic forces (Sarid, 1991; Güntherodt et al., 1995), it is more appropriate to denote those near-field microscopies which are based on the detection of forces by Scanning Force Microscopy (SFM).

3.1 Force Sensors

The general set-up in SFM is absolutely according to what has been discussed in Sect.2. In order to detect local forces or closely related physical quantities the sharp probe scanning the sample surface at some distance has to be linked to some sort of force sensor. A convenient

way to precisely measure forces is to convert them into deflections of a spring according to Hooke's law:

$$\Delta z = \frac{\Delta F}{c}, \tag{5}$$

where the deflection Δz is determined by the acting force ΔF and the spring constant c.

(a)

(b)

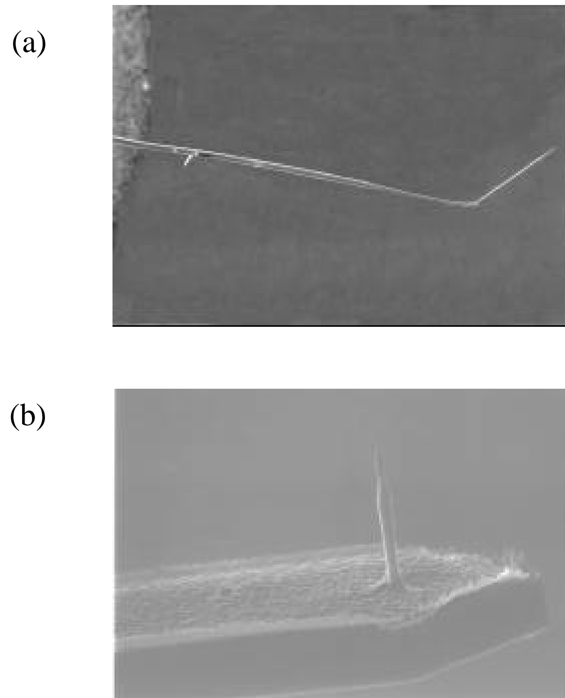

Fig. 2: *(a) Wire cantilever, fabricated by electrochemical etching and bending. (b) Micro-fabricated Si cantilever with integrated tip.*

In SFM the force-sensing spring consists of a miniaturized cantilever beam clamped at one end and equipped with the probing tip at the other end. While at the beginning tiny pieces of thin metal foils were equipped with glued diamond tips (Binnig et al., 1986), electrochemically etched metal wires (Fig. 2) were subsequently found to be easier to handle (Lemke et al., 1990). The increasing demand for cantilevers with integrated sharp tips, tailored reproducibly, and for the availability of a large number of them soon led to the development of microfabrication techniques based on the machining of Si-related materials (Albrecht et al., 1990 a) (Fig. 2). Today a variety of cantilevers with different geometries (mainly bar- and V-shaped) and with pyramidal as well as conical tips is commercially available.

The resonant frequency of a spring with spring constant c and lumped effective mass m is given by

$$\omega_0 = \sqrt{\frac{c}{m}} \,. \tag{6}$$

According to Eq. (5) it is desirable to have a low spring constant in order to achieve maximum force sensitivity. This is, however, contradicted by three aspects: First, according to Sect. 2 the spring constant should be a maximum in order to achieve via Eq. (6) a maximum resonant frequency, and thus a minimum vibrational sensitivity and a maximum scan rate. Second, the ultimate sensitivity of the force measurement is restricted by the thermal excitation of the cantilever. This latter quantity can be determined from the equipatition theorem (Heer, 1972):

$$(\Delta z)_{rms} = \sqrt{\frac{kT}{c}} \,, \tag{7}$$

where $(\Delta z)_{rms}$ is the rms displacement amplitude of the end of the cantilever due to thermal excitation. Third, if the cantilever is subject to a long-range attractive force, and this will almost always be the case upon probe-sample approach (see Sect. 3.3), its position becomes unstable if the magnitude of the force gradient equals the cantilever's spring constant (Landman et al., 1990). Thus, a certain minimum spring constant is needed in order to approach the sample sufficiently closely without a jump to contact.

In order to estimate the order of magnitude which the spring constant of the cantilever could have, it is straightforward to match c to the respective constant of interatomic coupling in solids (Rugar and Hansma, 1990). Taking in Eq. (6) $m = 10^{-25}$ kg and $\omega_o = 10^{13}$ Hz for atomic masses and vibrational frequencies one arrives at c = 10 N/m. Even smaller spring constants can be easily obtained by minimizing the cantilever's mass. Commercial cantilevers have a typical spring constant in the range of 10^{-2} N/m $\leq c \leq 10^{2}$ N/m, typical resonant frequencies in the range of 10 kHz $\leq \omega_0 \leq$ 500 kHz, a radius of curvature of the probing tip as small as 10 nm, and are usually fabricated of Si, SiO_2, or Si_3N_4.

If one again takes the above estimate for the interatomic coupling (c = 10 N/m) for a rough estimate of the resulting deflection of a cantilever which is subject to an interatomic interaction, one finds according to Eq. (5) that a force of 1 nN causes a deflection of 1 Å while thermal rms noise according to Eq. (7) amounts to about 20 % of this value. Thus, the task is to precisely measure cantilever deflections being smaller than 1 Å

In the first AFM approaches this was achieved by operating a complete STM on top of the cantilever (Binnig et al., 1986). Since this was not very reliable, numerous schemes based on optical interferometry involving homodyne (McClelland et al., 1987, Erlandsson et al., 1988 a, den Boef, 1989) and heterodyne (Martin et al., 1987) detection methods and differential techniques were presented between 1987 and 1989. The most successful interferometric scheme today is the fiber-optic approach (Rugar et al., 1988/89; Mulhern et al., 1991) shown in Fig. 3. The interference takes place between the cleaved end of a single-mode optical fiber and the cantilever. By employing a bidirectional fiber coupler the measured interference signal can be related to a reference signal thus minimizing the sensitivity to external noise sources or intensity and mode fluctuations of the diode laser.

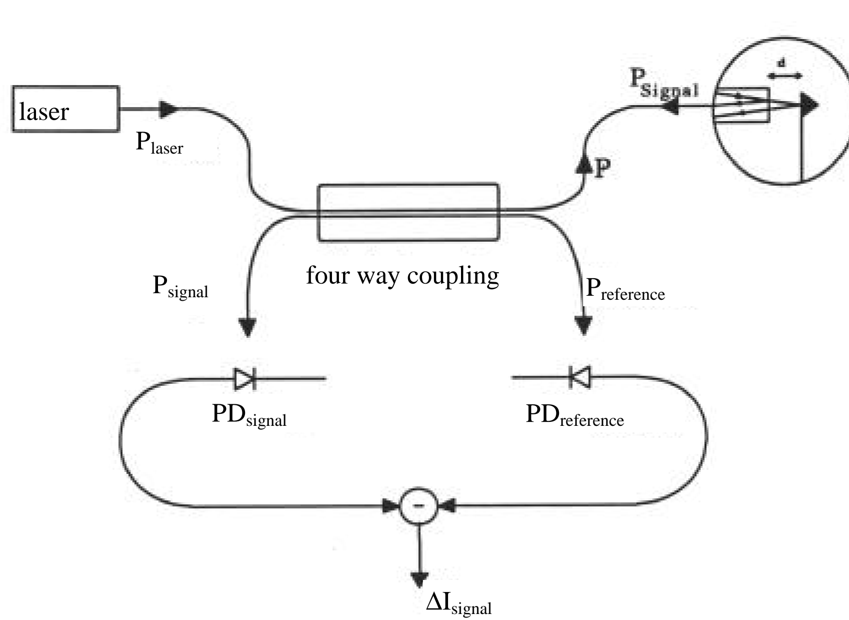

Fig. 3: *Set-up of the fiber-interferometric force microscope.*

A set-up which is even more easy to handle is the beam-deflection scheme (Meyer and Amer, 1988; Alexander et al., 1989; Ducker et al., 1990) shown in Fig. 4. The cantilever deflection is measured by detecting the related displacement of a laser beam reflected off the back of the

cantilever. Spatial variations of the reflected laser beam are detected by a position-sensitive photodetector, segmeted into four quadrants.

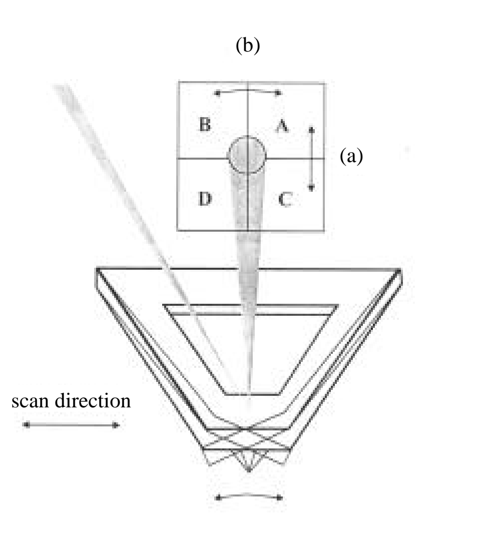

Fig. 4: *Beam-deflection set-up for the simultaneous detection of lateral and vertical force components.*

If the light beam moves between the upper and lower pairs of segmets the deflection of the cantilever can be deduced from a proper treatment of all individual photocurrents:

$$\Delta I_{vertical} = \left(I_{upper\ left} + I_{upper\ right}\right) - \left(I_{lower\ left} + I_{lower\ right}\right). \qquad (8)$$

$\Delta I_{vertical}$ is related to the deflection of the laser beam which is given by

$$\Delta y = \frac{d}{e} \Delta z , \qquad (9)$$

where l is the length of the cantilever and d that of the light path subsequent to reflection. Usually the laser beam has a Gaussian intensity prifile with a characteristic spot diameter increasing proportional to the distance d between cantilever and photodetector. The photocurrent generated in the detector is proportional to the flux density j of the photons hitting the photodiode:

$$\Delta I_{vertical} \propto \Delta y \, d \, j \, . \tag{10}$$

Since $j \propto 1/d^2$, insertion of Eq. (9) into Eq. (10) shows that $\Delta I_{vertical}$ is independent of the separation d between cantilever and detector. This is, however, valid only as long as the deflection Δy is small compared with spot diameter of the laser beam. For larger deflections nonlinearities in $\Delta I_{vertical}$ (Δy) result. The independence of the force sensor's sensitivity of the separation of photodetector and cantilever allows the realization of very compact beam-deflection schemes.

If a cantilever as shown in Fig. 4 is scanned in mechanical contact across a sample surface, the surface corrugation does not only cause vertical deflections but also a tiny twisting of the cantilever (Mate et al., 1987). This twisting obviously results in a horizontal deflection of the laser spot on the surface of the photodetector:

$$\Delta I_{horizontal} = \left(\Delta I_{upper\ left} + \Delta I_{lower\ left}\right) - \left(\Delta I_{upper\ right} + \Delta I_{lower\ right}\right). \tag{11}$$

In standard topographical imaging the occurance of lateral forces acting on the probing tip is often unwanted because the forces affect the images usually in a complex way (den Boef, 1991). Triangular cantilevers, which are commercially available as standard products were originally intended to minimize the torsion effects. However, from careful analysis of a huge amount of experimental data, one has realized that the analysis of lateral forces opens a new avenue in force microscopy.

Lateral Force Microscopy (LFM) allows the probing of friction forces between probe and sample at the nanometer or even at the atomic scale. Since there are a lot of open questions related to friction phenomena and their microscopic origin, LFM has gained much importance over the past years. Unfortunately, it is not straightforward to calculate the actual lateral force acting on the probing tip from the current difference in Eq. (11) (Baumeister and Marks, 1967). Thus, absolute values from a sample surface are usually only obtained by first experimentally calibrating the force sensor on suitable reference systems.

In order to make the beam-deflection set-up unsensitive to external perturbations or fluctuations of the laser diode the ratios $\Delta I_{vertical}/\Delta I$ and $\Delta I_{horizontal}/\Delta I$, with ΔI being the sum of all individual photocurrents, are taken for data aquisition. An optimized beam-deflection set-up is then practically almost as sensitive as the interferometer scheme shown in Fig. 3. Beam deflection offers the advantage of being capable of detecting simultaneously lateral and vertical forces. The mechanical set-up can be kept relatively simple. The fiber interferometer is by far more versatile. It can be implemented under UHV or, e. g., under low-temperature conditions. A disadvantage is, however, the more complex mechanical set-up which allows relative positioning of cantilever and fiber and the restriction to vertical forces.

In comparison with beam deflection and fiber interferometry, the above mentioned alternative optical deflection sensors as well as capacitance sensors (Göddenhenrich et al., 1990; Neubauer et al., 1990) or SQUID-based magnetic detection (Dworak et al., 1997) can be considered as more or less exotic or at least as not widely used. These approaches, however, often represent the absolute state of the art with respect to the obtainable sensitivity.

Apart from beam deflection and fiber interferometry there is one more very elegant and commercially applied approach (Tortonese et al., 1991). Piezoresistive cantilevers change their electrical conductivity due to tiny deflections. Force measurements can thus simply be performed by probing the actual resistance of the cantilever, preferentially in a bridge set-up. A particularly high sensitivity is obtained if the force microscope is operated in the dynamic mode (see Sect. 3.6). The wide employment of piezoresistive cantilevers is presently restricted by their limited commercial availability. In future, also piezoelectric cantilevers (Itoh and Suga, 1993) may gain some importance. Several groups are presently working on their optimization.

Apart from further developing schemes to sensitively detect cantilever deflections also some progress has been made in further improving the monolithically integrated tip of the cantilever. In many applications the sharpness of this tip determines the obtained lateral resolution. Possibilities to increase the sharpness involve ion etching and local electron-beam-induced deposition of material. Using the latter approach ultrasharp contamination tips consisting of carbon and carbon compounds can be grown in a scanning electron microscope on top of the monolithical tip of the cantilever (Fig. 5). Tip diameter and aspect ratio can well be con-

trolled. A disadvantage of all presently employed tip-refinement methods is, however, that they rule out batch fabrication.

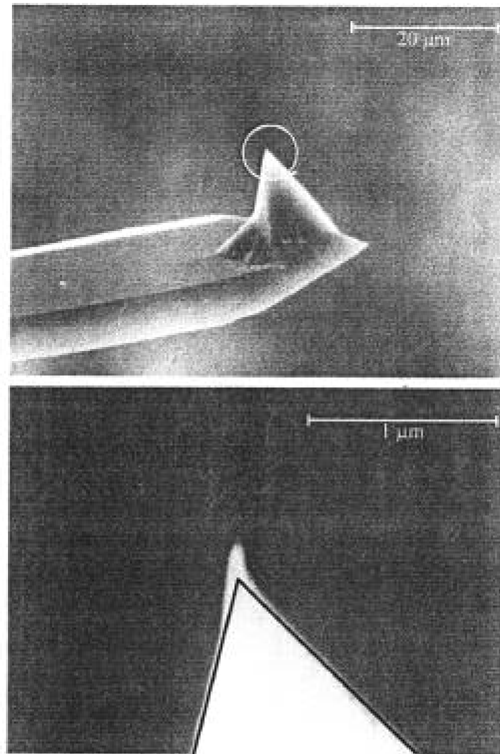

Fig. 5: *Electron-beam deposited "supertip" on top of an ordinary Si probe.*

3.2 State-of-the-Art Set-Ups

A maximum versatility of a force microscope is given if the instrument can be operated under various different environmental conditions frequently met in standard experiments in solid-state or soft-matter research. Such a set-up is shown in Fig. 6 (Euler et al., 1997).

The force microscope is based on the fiber-interferometric scheme shown in Fig. 3. It can be operated under standard ambient conditions, in a gas atmosphere, in UHV, with the sample immersed in a liquid, or upon being inserted in a cryostat containing cold helium exchange gas, or even liquid helium. Such a manifold applicability requires a remote control of all movable parts and a highly sophisticated design largely avoiding residual thermal drift of mechanical components.

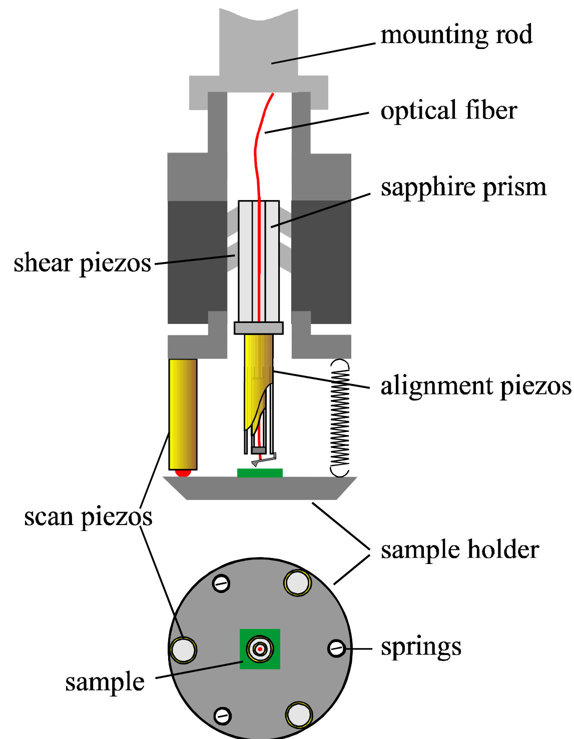

Fig. 6: *Schematics of the set-up of a versatile fiber-interferometric force microscope (Euler et al., 1997).*

According to the basic considerations in Sect. 2 adjustment of the microscope requires in this case coarse and fine approaches of fiber end and cantilever on the one hand and of cantilever and sample on the other hand. This task is solved by a combination of different piezoelectric actuators involving two concentric piezo tubes for fiber and cantilever positioning, a motor driven by shear piezos for positioning of the probe with respect to the sample, and an arrangement of three piezo tubes for scanning (Besocke, 1987). Since the set-up does not contain any element which could only be adjusted manually, fine tuning of the interferometer or the probe-sample separation within a cryostat or a UHV-chamber is straightforward. The piezoelectric "walker" can move stepwise over a few millimeters exhibiting a single-step precision of 100 nm or less. Since the whole microscope head is made from nonmagnetic components, it can be operated under the influence of high magnetic fields.

If SFM should be performed on liquid/solid interfaces, the sample holder in Fig. 6 is substituted by an "electrochemical cell" (Siebel et al., 1997). This device contains a couple of reference electrodes and is chemically largely inert. Sample, cantilever and fiber end are all immersed in the liquid environment. A considerable strength of the fiber interferometer is that no

interference between light reflected off the cantilever on the one hand and at the liquid/gas (or liquid/air) interface on the other hand affects the measurement. Such an interference is often a problem in beam-deflection set-ups.

Upon UHV operation it is necessary that probes and samples can be exchanged *in situ*. This task is solved by suitable mechanical manipulators which are standard equipment in UHV technology. A complex multi-chamber UHV system with facilities for sample preparation, general-purpose analysis, and with the possibility to perform scanning electron microscopy (SEM), STM and AFM investigations is shown in Fig. 7 (Memmert et al., 1996).

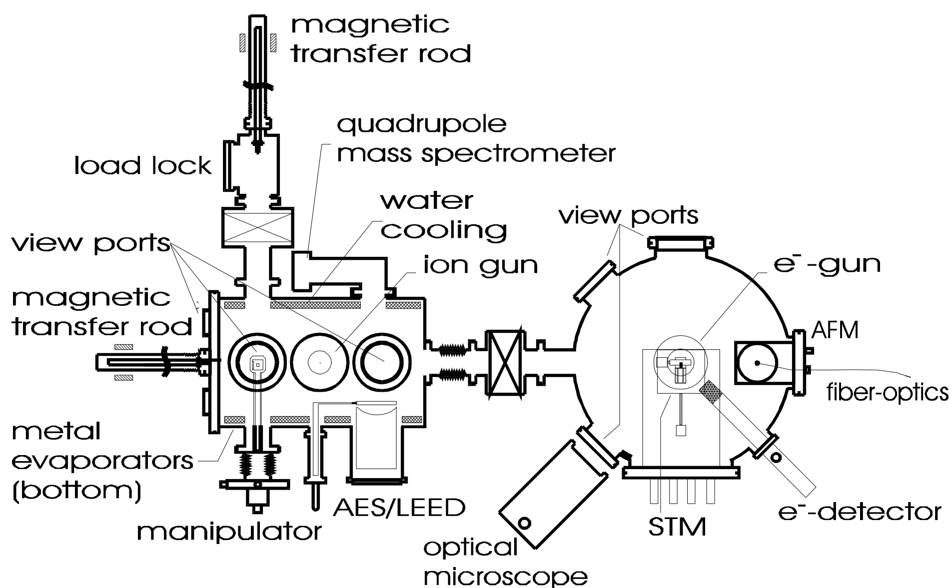

Fig. 7: *Multipurpose UHV chamber for thin film preparation and analysis. The set-up involves an optical microscope, a scanning electron microscope, a scanning tunneling microscope, and an atomic force microscope attached to the analysis chamber. The preparation chamber contains standard components for global surface analysis (Memmert et al., 1996).*

Even more complex are set-ups which additionally allow a variable sample temperature involving low and elevated values. Some groups are presently developing such set-ups. The most sophisticated approaches offer the option to additionally apply high magnetic fields. Often one microscope head can be employed to either perform STM or AFM operation. Commercial solutions will certainly be available in the near future.

3.3 Probe-Sample Interactions

If two solids are in close proximity to each other a manifold of interactions manifesting themselves in forces can result. The sensitivity of state-of-the-art force microscopes is well suficient to detect surface forces at a nanometer scale and even intermolecular interactions (Israelachvili, 1985). Figure 8 shows the typical variation of the interaction potential between probe and sample if their separation is successively decreased.

At relatively large separations, typically of the order of 1 nm or more, van der Waals interactions lead to a negative interaction potential and thus to attractive forces (Hartmann, 1990/91). These forces are ever present in any environmental situation. Their origin are zero-point quantum fluctuations which sensitively depend on the local probe-sample geometry, on the involved materials, and on the medium being intervenient between probe and sample. The van der Waals forces usually increase in magnitude if the probe approaches the sample surface. Often the resulting force-distance curve can be characterized by a simple reciprocal power law (Hartmann, 1994). If the outermost atom of the probe starts to penetrate the sample surface, i. e., if the electronic wave functions of probe and sample start to overlap, short-range repulsive forces are introduced. Since the valence- and conduction-band electrons are typically 1-10 Å away from the outermost atomic nuclei of the sample, while the extent of the inner bound electrons is 10-30 pm, the resulting repulsion is indeed very short-range. Upon further approaching the probe to the sample more and more interatomic interactions lead to a continuously increasing repulsion, while the overall long-range probe-sample interaction is still attractive. Thus the net interaction potential exhibits first a point of inflection, then an absolute minimum, followed by a situation where the repulsive short-range interactions just balance the attractive long-range interactions, and finally a regime where ultimately the repulsive interactions dominate the attractive ones. In this regime the probe seriously penetrates the sample, first leading to elastic and finally to inelastic deformations.

The above scenario occurs for any given experiment since it represents the general behavior of two solids brought into sufficiently close proximity. However, a couple of additional interactions can result if suitable environmental conditions are chosen or if external manipulations are undertaken in a suitable way. If, e. g., an electrical potential is applied between probe and

sample, Coulomb interactions provide an additional long-range attractive contribution. Charges of equal sign on probe and sample would in contrast lead to repulsive forces. If probe and sample consist of ferromagnetic materials the resulting long-range magnetostatic interactions can either be repulsive or attractive. In any case the situation is still relatively simple since all mentioned long-range interactions, i. e., van der Waals, Coulomb, and magnetic dipole forces can be treated in terms of a linear superposition.

Linear physics breaks down if the sample surface is a solid/liquid interface. This situation is not so uncommon because sample surfaces are frequently covered by thin adsorbed water or other quasi-liquid contamination layers when subject to ambient conditions. The same holds of course for the cantilever probes. The presence of liquid thin films or even only of a sufficiently high humidity manifests itself in the formation of a liquid capillary between probe and sample. The meniscus causes huge attractive interactions usually dominating all interactions of interest mentioned above (Hartmann, 1994). The problem is not only that capillaries cause large "background forces". A more serious consequence is that the overall loading force exerted by the probe on the sample is greatly increased. This limits the obtained lateral resolution in contact-mode SFM and sometimes even leads to destructions of the sample surface (Sect. 3.4). Additionally, liquid menisci are sources for pronounced hysteresis effects in force curves (Sect. 3.8).

There are two possibilities to avoid capillary formation. The straightforward one is to perform the AFM experiment under UHV conditions. This reduces the adsorption of contaminants to a minimum and allows in many cases the analysis of locally absolutely clean surfaces over some time. The second possibility which excludes liquid meniscus formation between probing tip and sample is to completely immerse cantilever and sample in a suitable liquid. This approach offers a broad avenue of new applications of SPM (Gewirth and Siegenthaler, 1995). The main reason for this is that the surfaces of sample and cantilever become solid/liquid interfaces.

A solid/liquid interface represents characteristic properties of the solid and of the adjacent liquid. It generally also involves, however, special physical and chemical phenomena which only result if the selected solid is in contact with the selected liquid. In any case the presence of the liquid immersion changes especially the aforementioned long-range interactions, except

the magnetostatic forces. Both Coulomb and van der Waals forces sensitively depend upon the dielectric properties of the liquid in the intervening gap between probe and sample. For the electrostatic force F this dependence is given by $F \propto 1/\varepsilon$. In the case of van der Waals forces the relationship is much more complicated because the interaction depends on the actual static and dynamic dielectric properties of probe, sample, and immersion liquid (Hartmann, 1994). The most striking consequence of the complex relation between van der Waals interactions and electrodynamic properties - especially in the ultraviolet part of the spectrum - is that a repulsive interaction can occur, while van der Waals forces in vacuum or air are always attractive. Thus, an immersion liquid can be used to avoid capillary formation and to lower the magnitude of van der Waals forces. One should of course be aware of the possibility that the behavior of the liquid/solid interface can deviate considerably from that of the free sample surface.

One such deviation results from solvation forces which manifest themselves if liquid molecules are squeezed between probe and sample being at very close proximity to each other (Hartmann, 1994). Other liquid-induced phenomena involve the relevance of hydrophilicity or of hydrophobic effects. The most important point, however, is that an immersion liquid can contain a well-defined concentration of positive and/or negative ions, eventually under electrical potential control. In this case one has an electrochemical environment. For such an environment it is well known that double-layer forces, i. e., ionic Coulomb forces, play an important role. The range of these repulsive forces depends on the valence and concentration of the ion species but also on the electrical surface potential. Utilizing an electrochemical environment, one can on the one hand well control the forces upon imaging a sample and one can on the other hand perform electrochemical investigations at the nanometer scale.

It was mentioned above that linear approaches in the characterization of probe-sample interactions often break down if a liquid immersion medium is present. The reason for this now becomes obvious: Especially van der Waals forces, double-layer forces and solvation forces can not simply be superimposed in a linear way nor can they exhaustively be treated in a simple continuous theory. Strong local variations in the ionic or molecular concentrations which are present if double-layer and solvation forces exist result in the local dielectric behavior of the immersion liquid which strongly deviates from its bulk behavior. The local dielectric behavior, in turn, determines the van der Waals forces acting between probe and sample.

It seems worthwhile to emphasize that the presence of liquids as well as that of electro- or magnetostatic forces usually modifies the most simple variation of the probe-sample interaction potential shown in Fig. 8 significantly. This complicates data analysis, in particular, if various intermolecular and surface forces are present at the same time. On the other hand the manifold of interactions which can externally be stimulated offers a lot of special applications of SFM, like electrochemical, magnetic or electric force microscopy.

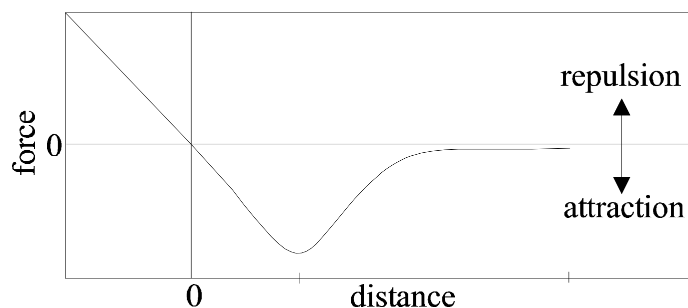

Fig. 8: *Typical variation of the force between probe and sample with their relative distance.*

3.4 Contact-Mode Operation

According to Hooke's law, Eq. (5), the cantilever which is raster-scanned across the sample surface exhibits a locally varying deflection which directly represents the corrugation of the sample surface. Since the force microscope is equipped with a feedback loop (Sect. 2) it is convenient to keep the actual cantilever deflection constant by suitably adapting the probe-sample separation continuously during scanning. Thus, the working distance is increased if the local force exerted on the cantilever becomes temporarily relatively high, and it is decreased if the force falls below a prechosen setpoint. The resulting *constant-force mode* is one of the most important modes in which a force microscope can be operated. The very first AFM observations have all been performed in this mode (Binnig et al., 1986). Since a proper feedback action which ensures constant forces between cantilever and sample is ultimately limited by the response time of the feedback circuit, the scan speed in the constant-force mode is evidently limited. In many cases, especially where only the nanoscale topography of the sample is of interest, an alternative mode of operation is to raster-scan the probe across the sample surface at a constant average height, where the cantilever deflection and thus the force is allowed

to change during scanning. The *variable-deflection mode* is achieved by limiting the feedback response to relatively low frequencies and by recording higher-frequency deflections as a function of probe position. Compared with the constant-force mode significantly higher scan rates can be achieved in the variable-deflection mode. Since, however, the recorded maps do not represent exact equiforce surfaces the recorded data are generally more difficult to interpret. It is thus convenient - if not necessary - to ensure that relative variations of the force do not exceed a few percent for the whole recorded image.

It is important to note that the term *contact mode* is at first sight not very well defined. For example, STM is usually considered as a noncontacting, nondestructive imaging method, where a wave-function overlap between one atom of the tip with locally one atom of the sample surface is utilized to obtain local information. In contrast, one would intuitively think about a mechanical contact if the outermost atom of a cantilever tip starts to overlap with a sample atom resulting in repulsive forces between the two interacting atoms. Thus, one certainly has to define more precisely what is denoted by *contact-mode force microscopy*. Basically this mode is very similar to the working principle of Edison's gramophone or of a classical stylus profilometer (Williamson, 1967/68). While, however, for the latter instrument even in the most advanced set-ups the force exerted by the stylus tip on the sample is of the order of 10^{-4} N, typical values in force microscopy are much smaller. It is most instructive to discuss image formation in the contact mode with the help of Fig. 8. The feedback setpoint for an operation in the constant-force or variable-deflection mode is chosen within the regime of overall repulsive interaction. This means the probe exerts a certain loading force on the sample surface. In order to keep this loading force either locally absolutely constant or constant in average during scanning, the probe has to follow the atomic or nanoscale corrugation of the sample surface. In this way it is possible to obtain images like those shown in Fig. 9 and 10.

It has been demonstrated that atomic-scale periodicities can well be resolved by AFM in the contact mode on layered materials, on ionic crystals, and on metals. Typical loading forces are of the order of 10^{-8} - 10^{-7} N. Experimentally accessible is a cantilever deflection which can be converted according to Eq. (5) into a net force. It is important to emphasize again that this experimentally determined force is composed of a long-range attractive interaction between probe and sample and a short-range repulsive interaction between the outermost probe atoms and the sample surface. Consequently, if the force setpoint in contact-mode AFM is given by a

certain value, e. g., 10^{-8} N, which represents a net repulsive interaction, the corresponding repulsive force exerted by atoms at the probe apex on the sample is much higher than the set-point value. Since typical atomic binding forces exhibit a magnitude of the order of 10^{-9} N (Sect. 3.1) it is evident that a loading force of the order of at least 10^{-8} N leads to local deformations or even destructions of the sample surface and eventually of the probe apex. Such deformations lead to an increase of the contact radius. An increase of the contact radius in turn leads to a reduction of the force acting per atom between probe and sample. The increasing extent of the contact radius is the mechanism which largely avoids irreversible perturbations of sample and probe in the imaging process.

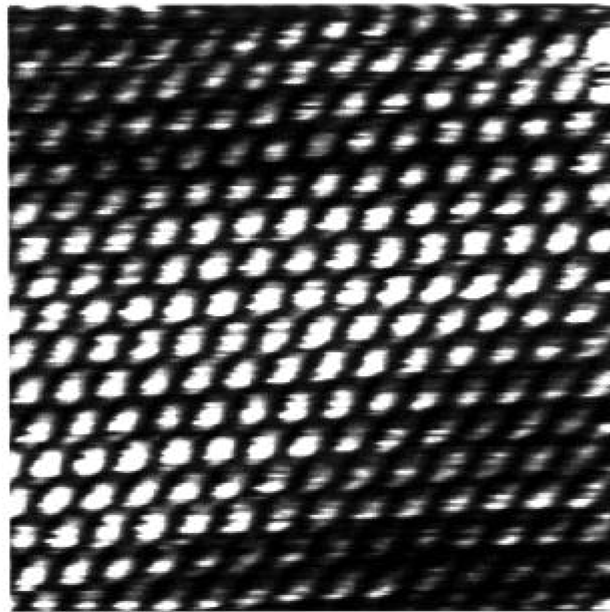

Fig. 9: *Atomic-scale resolution on Au(111) in the constant-force contact mode. The scanned area is 4 nm x 4 nm (courtesy by P. Güthner, Omicron Vakuumphysik).*

On the one hand, the force per atom for a relatively large contact radius is sufficiently small to not cause surface damage. On the other hand, a large contact radius only exists if the probing tip is a multi-atom tip rather than a single-atom one. This latter conclusion than rises the serious question how an obviously atomic resolution like that shown in Fig. 9 could be obtained if many atoms of probe and sample do interact. An important hint towards an answer of this question is that almost all of the experimental data acquired in the high-resolution contact mode of operation only exhibit an *atomic periodicity* rather than a *true atomic resolution*. This means that generally only the periodic arrangement of unit cells is detected but neither the inner atomic configuration of this unit cell nor individual atomic lattice defects. Both features

are, however, generally observed in STM images. There are two mechanisms being responsible for the majority of pseudoatomic-resolution observations. Moiré interference patterns of atomic periodicity result if the probe's atomic lattice glides across the sample's atomic lattice. Additionally, for layered materials such as graphite or mica the probing tip often carries a piece of sample material picked up during scanning (Abraham and Batra, 1989; Gould et al., 1989). In contrast, on ionic crystals such as LiF, NaCl, and AgBr a preferential imaging of the larger negatively charges ions would explain why an atomic periodicity but never an individual atomic lattice defect is visible (Meyer and Amer, 1990; Meyer et al., 1991). The discussed multi-atom imaging mechanisms emphasize once more that true atomic resolution in contact-mode AFM requires ultrasmall loading forces as a prerequisite for a single-atom probe. These can generally not be achieved under ambient conditions (Binnig, 1992).

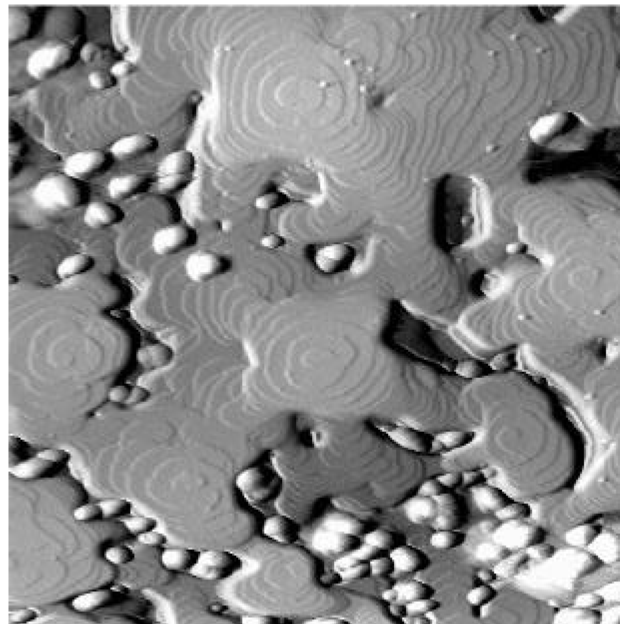

Fig. 10: *Contact-mode image taken at a temperature of 7.8 K. The sample is* $YBa_2Cu_3O_{7-d}$ *sputter-deposited on a* $SrTiO_3$ *substrate. The image clearly shows that the superconducting film is composed of screw dislocations. The imaged area is 800 nm x 800 nm.*

It is important to look what theory tells us about the contact-mode imaging mechanism. The key to model the actually occurring forces is the electrostatic Hellman-Feynman theorem (Deb, 1973). According to this theorem the probe-sample interactions can be ultimately obtained from classical electrostatics once the electronic wave functions of probe and sample

surface have been determined by an accurate quantum-mechanical calculation. The latter is, however, the major problem. Numerical approaches (Ciraci et al., 1990) indicate that there are two relevant contributions to the interatomic forces. A very short-range repulsive interaction with a strong distance dependence results from the Coulomb force between the atomic nuclei of probe and sample. Thus contact-mode AFM can be assumed to predominantly probe the position of atomic nuclei at the sample surface in contrast to STM which probes the local density of electronic states close to the Fermi level. The second contribution to the total interatomic interaction results from an attractive Coulomb force between the electron clouds of the probe and the atomic nuclei of the sample and vice versa. This contribution is of longer range than the aforementioned ones and does not decay so rapidly with increasing probe-sample distance. If AFM could be performed right within that tiny probe-sample distance regime, where the attractive interatomic interaction dominates the repulsive ones, it would probe primarily the total electronic density of states at the sample surface. This is then more closely related to what STM probes. The difference is, however, that the latter technique is restricted to near-Fermi level electronic states.

3.5 Lateral Forces

Friction is a well-known phenomenon occurring whenever two bodies in contact are in relative motion with respect to each other. The basic fundamentals of this phenomenon are not very well known and the theory of friction is largely phenomenological. It is obvious that a macroscopic friction force F_f is ultimately related to the microscopic structure of the contact area between the two bodies which are in direct mechanical contact. Since all surfaces are rough, at least at a microscopic scale, the actual contact area is given by relatively few exposed sites establishing a mechanical contact between the two bodies in terms of dominating repulsive forces (Sect. 3.3). The total frictional force is then proportional to the actual contact area A composed by summing up all microscopic contact sites:

$$F_f \propto A\,. \tag{12}$$

It has already been discussed (Sect. 3.4) that an increasing loading force F_l leads to an increasing number of microcontacts and thus to a proportionally increasing total contact area:

$$A \propto F_l \,. \tag{13}$$

The combination of Eqs. (12) and (13) yields Amontons' well-known law,

$$F_f = \mu F_l \,, \tag{14}$$

which relates the frictional force to the loading force by the friction coefficient μ and which implies that F_f is independent of the interface area between the two contacting bodies. μ is a phenomenological quantity being characteristic for the involved materials.

It is obvious that AFM is a very well-suited method to analyze friction at an atomic or a nanometer scale because the loading force can be varied over a large range, thus permitting a variation of the probe-sample contact radius in the range of one atom up to more than 100 nm (McClelland, 1989; McClelland and Cohen, 1990). LFM as a special application of contact-mode AFM is thus extremely interesting for both the analysis of the microscopic foundations of friction and the imaging of surfaces which exhibit only minor topographic variations but pronounced variations in the chemical composition of the surface. Lateral forces are measured in detecting the cantilever torsion as indicated in Fig. 4. The typical hysteresis obtained by recording this torsion upon scanning the cantilever forward and backward across the sample is shown in Fig. 11. The hysteresis loop is mainly caused by the static friction becoming effective if the scan direction changes. If the loading force is decreased, static friction also decreases leading to a decreasing loop size.

Even atomic-scale friction can be successfully observed (Mate et al., 1987). Sliding of the probe was found to be nonuniform, exhibiting a pronounced stick-slip motion. Slips take place instantaneously, while in between probe and sample temporarily stick together. A resulting periodicity coincides with the lattice periodicity of the sample surface. This means that the atomic arrangement of probe and sample surfaces determines in a measurable way the frictional properties of the probe-sample interface. The atomic-scale variation of friction can indeed be used for high-resolution imaging (Fig. 12).

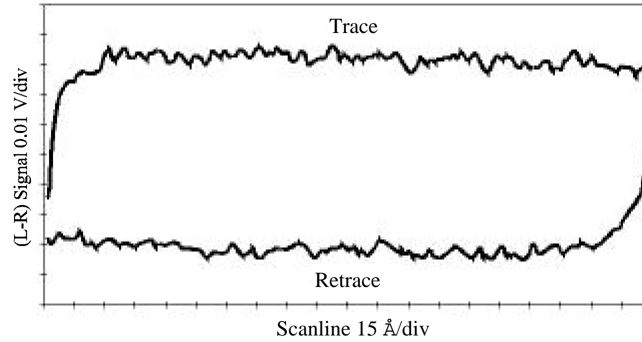

Fig. 11: *Lateral force variations along opposite scans on a glass substrate.*

LFM has been performed on a large variety of samples and has proven capable of providing important information especially on local variations in chemical composition. Studies with the aim of exploiting the microscopic origin of friction were concentrated mainly on layered materials such as graphite or mica. For the latter material the frictional force varies with the periodicity of the hexagonal layer of SiO_4 units (Erlandsson et al., 1988 b). The atomic-scale stick-slip behavior was also found in molecular dynamics simulations concerning a reactive probe-substrate ensemble where scanning was assumed to be performed under constant loading-force conditions (Landman et al., 1989 a, b).

A question of fundamental interest is, of course, if the coefficient of friction μ in Eq. (14) as determined in the conventional way is the same as that which can be estimated from LFM experiments. A glance to Fig. 11, however, shows that the frictional force obtained at a certain constant loading force varies along the surface scan. These variations are related to the nanoscale or atomic surface structure. Consequently, μ has to be defined as some average value. Numerous measurements on a large variety of materials have shown that in general this average value is not in accordance with the macroscopically determined coefficient. A frequent observation is a more or less pronounced dependence of the microscopic value for μ on the loading force or, in other words, a nonlinear relationship between F_f and F_l. This behavior which is in contradiction to Eq. (14) is supported by first-principles theories of atomic-scale friction (Zhong and Tománek, 1990).

LFM is a special variant of contact-mode AFM. Thus the above considerations concerning true atomic resolution and nondestructiveness also hold for frictional force imaging. Additionally it is difficult to determine absolute forces from the measurements due to the relatively

complex response of the cantilever to torsion. It can, however, be estimated from a large amount of experiments that the typical magnitude of lateral forces is in the range of 10^{-10} - 10^{-8} N for loading forces which do not cause remanent perturbations of the sample surface.

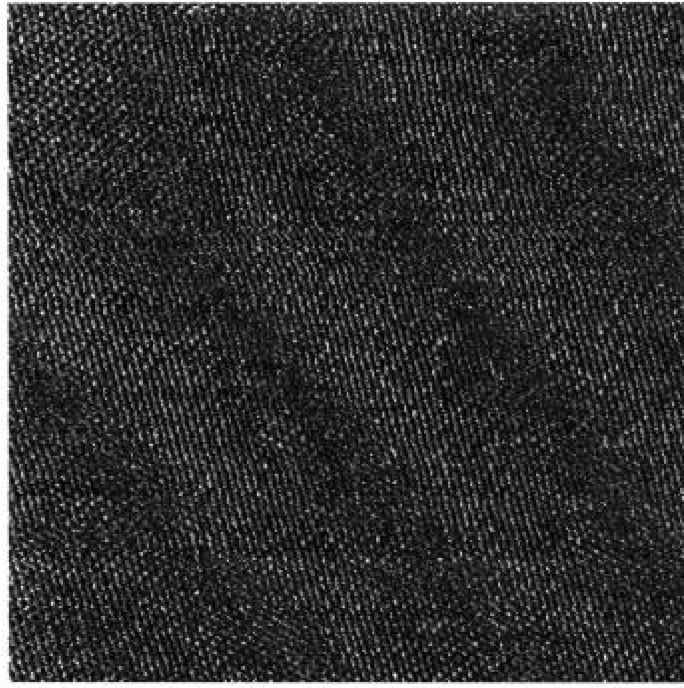

Fig. 12: *Atomic-scale friction on the 23 x $\sqrt{3}$ reconstruction of Au(111). The imaged area is 24 nm x 24 nm (courtesy by P. Güthner, Omicron Vacuumphysik).*

3.6 Noncontact-Mode Operation

It is evident that when lifting the probe by at least one nanometer from the sample surface only long-range interactions remain. According to what has already been discussed (Sect. 3.3) the relevant forces result in general from van der Waals interactions, electro- and magnetostatic interactions, and, under ambient conditions, often from the formation of liquid capillaries. Information of the atomic or nanoscale surface structure gets completely lost. While van der Waals forces are relatively small and capillary forces can be avoided by either choosing a sufficiently large working distance or by working on clean surfaces, electro- and magnetostatic interactions can yield relatively strong forces. This provides important information about the electrical or magnetic charge distribution in the near-surface regime of the sample. Since these charge distributions can be manifold, the lateral variation as well as the range of the resulting interactions are very different on different samples. Near-field

the resulting interactions are very different on different samples. Near-field operation means in this context that only charges in probe and sample within a certain volume around the probe apex contribute to contrast formation. In other words, if the static interaction is modeled in terms of a multipole expansion of the charge distribution, one usually finds monopole, dipole, and higher contributions which all have to be taken into account up to a certain degree. Thus, for the magnetostatic interaction it is very frequently found that the resulting forces are not simply dipole forces but that the monopole term dominates contrast formation (Hartmann, 1994).

Especially if the microscope is operated in the noncontact mode it is not very reasonable to denote this by *AFM* and the acronym *SFM* should clearly be preferred. One of the most important variants of noncontact SFM is certainly Magnetic Force Microscopy (MFM), especially for applied research purposes (Hartmann et al., 1991). In order to image magnetic domains or even interdomain boundaries, a microfabricated cantilever like that shown in Fig. 2. is coated with a magnetic thin film. When subject to the surface stray field of a sample the resulting magnetostatic interactions then provide information about the surface magnetization of the sample. One has, however, to keep in mind that stray field and magnetization are in general related in a complex way. On the other hand, stray-field mapping sometimes permits a clear information on the magnetic domain structure as in Fig. 13. A spatial resolution much below 100 nm can be reached routinely (Hartmann, 1994).

In the beginning (Martin and Wickramasinghe, 1987; Sáenz et al., 1987) MFM was mainly used to investigate components of the magnetic recording technology. A large amount of work (Rugar et al., 1990) has strikingly confirmed the usefulness of the technique in applied research. The first image of an interdomain boundary (Göddenhenrich et al., 1988) was a further breakthrough and made MFM also highly interesting for basic research. The main strength of MFM in comparison with other magnetic imaging methods is that the investigations can be performed under ambient conditions with only little or no surface preparation. MFM has not only successfully been applied to ferromagnetic materials but also to the imaging of vortices in superconductors (Moser et al., 1995). A further important field of application is the analysis of magnetic stray fields caused by electrical currents (Göddenhenrich et al., 1990 b; Hartmann, 1994). Since other well-established techniques only probe local variations of the elec-

trical potential the application of MFM in semiconductor chip analysis will be of growing importance.

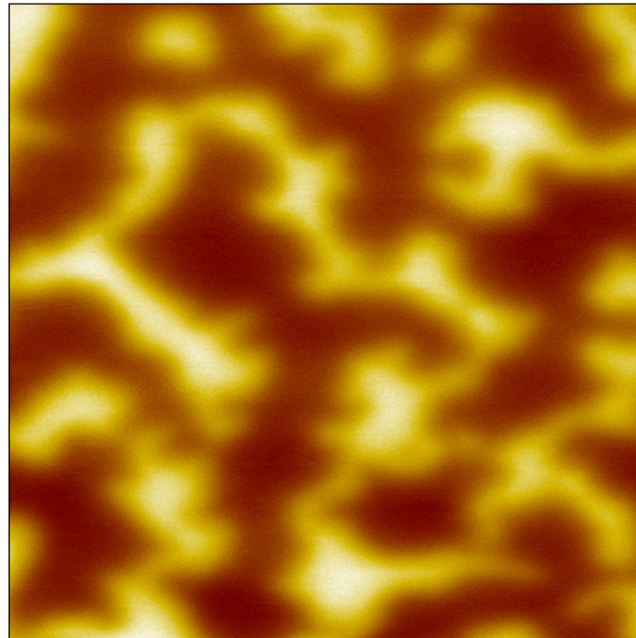

Fig. 13: *MFM image of a $Tb_{30}Fe_{62}Co_8$ thin film showing the demagnetized-state domain configuration in the material. The scanned area is 5 µm x 5 µm.*

In Sect. 3.4 it was already pointed out that contact-mode force microscopy involves the danger of destructiveness if the loading force becomes too high. In spite of the relatively large probe-sample separation MFM also involves the potential for sample perturbation. If the stray field produced by the probing tip is too high the magnetization of the sample can be affected during scanning (Hartmann, 1988). This phenomenon was found in a number of measurements on soft magnetic samples and was successfully modeled in micromagnetic simulations (Scheinfein et al., 1990). There are two ways to circumvent the problem. First, it is possible to deposit a small magnetic particle right at the apex of the probe such that it looks like the tip shown in Fig. 5 (Leinenbach et al., 1997). Second, it is possible to utilize eddy-currents excited in a nonferromagnetic probe for completely nondestructive magnetic imaging (Hoffmann et al., 1997).

Electrical charges can be present in probe and sample either permanently or can be introduced by applying an electrical potential between probe and sample. Coulomb forces have been measured on a variety of samples (Martin et al., 1988; Stern et al., 1988; Terris et al.,

1989/90). One of the most striking demonstrations of the obtainable sensitivity in electric force microscopy is the monitoring of the incremental decay of a charge generated by a voltage pulse in Si_3N_4 (Schönenberger and Alvarado, 1990 a). Other experiments were concentrated on the study of contact electrification or triboelectrification, where in the latter case charges were produced by bringing the probe in contact with the sample without an externally applied bias voltage (Terris et al., 1989). A further important field of application of charge microscopy is the analysis of ferroelectric materials, where even individual domain walls have been imaged (Saurenbach and Terris, 1990).

If a potential difference V is externally applied between probe and sample, the resulting Coulomb force is given by

$$F_C = \varphi(d) V^2 . \tag{15}$$

φ depends on the geometry of the probe, on the local geometrical configuration of the sample surface, on the dielectric environment and explicitly on the probe-sample spacing d. If the probe-sample arrangement is modeled to a first order by a simple parallel-plate capacitor with an electrode area A involving a dielectric medium of relative constant ε_r, one would find $\varphi(d) = \varepsilon_o \varepsilon_r A / (2d^2)$. F_C exhibits a square dependence in the local electrical potential which opens the possibility to measure potential variations across sample surfaces. This is particularly interesting for, e. g., semiconductor devices (Martin et al., 1988; Abraham et al., 1991) and surface-conductance measurements in general (Morita et al., 1989). Furthermore, due to the dependence of φ on ε_r also dielectric properties of a sample surface can be measured which opens a large variety of applications. Finally, it has been demonstrated that it is very useful to apply a potential difference also for nonelectrical measurements in order to separate topographical influences from the long-range interactions of interest (Schönenberger and Alvarado, 1990).

So far one could get the impression that noncontact-mode operation simply consists in lifting the probe of the force microscope up to a certain probe-sample distance to measure the long-range interaction in terms of a static force. This is, however, the absolute exception. In discussing the mechanical properties of cantilevers (Sect. 3.1) mainly static characteristics have been addressed. It turns out, however, that a broad avenue of new possibilities is opened if the

dynamic properties of the probes are utilized in appropriate approaches (Binnig et al., 1986). As a first characteristic quantity describing these dynamic properties the resonant frequency was derived in Eq. (6).

Today, noncontact force microscopy usually involves a sinosoidal excitation of the cantilever with a frequency close to its main resonant frequency as calculated in Eq. (6). In order to excite the vibration of the probe, the cantilever can be attached, e. g., to a bimorph piezoelectric plate. Apart from the cantilever also the sample can be excited by a suitable piezoelectric actuator. In some applications it is convenient to externally modulate the long-range probe-sample interaction which also excites a cantilever oscillation. The latter possibility is in particular given if electric or magnetic interactions are involved. The noncontact mode of operation involving an oscillating cantilever is frequently also called the *dynamic* or *ac mode*.

In contrast to the detection of a quasistatic force the response of the cantilever in the dynamic mode is in any case more complex and deserves a more detailed discussion. If the cantilever is excited sinosoidally at its clamped end with a frequency ω and an amplitude δ_0 the probing tip likewise oscillates sinosoidally with a certain amplitude δ exhibiting a certain phase shift α with respect to the driving signal applied to the piezoelectric actuator. The deflection sensor monitors the motion of the probing tip provided that the bandwidth is large enough. The latter requirement clearly favours the optical deflection sensors discussed in Sect. 3.1. The equation of motion, the solution of which is monitored by the deflection sensor, is given by

$$\frac{\partial^2 d}{\partial t^2}+\frac{\omega_0}{Q}\frac{\partial d}{\partial t}+\omega_0^2\left(d-d_0\right)=\delta_0\,\omega_0\cos\left(\omega t\right), \tag{16}$$

where d_0 is the probe-sample distance at zero oscillation amplitude and d(t) the momentum probe-sample separation. Q is apart from the intrinsic properties of the cantilever, which are the lumped effective mass and the resonant frequency, determined by the damping factor γ:

$$Q=\frac{m\omega_0}{2\gamma}, \tag{17}$$

with ω_0 from Eq. (6). γ introduces the influence of the environmental medium which could be ambient air, a liquid, or UHV. Q thus ranges from values below 100 for liquids, air, or other gases at an appropriate pressure, to more than 100,000 which is sometimes obtained in UHV. After the usual building-up, Eq. (16) leads to the steady-state solution

$$d(t) = d_0 + \delta \cos(\omega t + \alpha) \tag{18}$$

for the forced oscillator. The amplitude of the probe's oscillation is given by

$$\delta = \frac{\delta_0 \omega_0^2}{\sqrt{\left(\omega^2 - \omega_0^2\right)^2 + 4\gamma^2 \omega^2}} \,. \tag{19}$$

The phase shift between this oscillation and the excitation signal amounts to

$$\alpha = \arctan \frac{2\gamma\omega}{\omega^2 - \omega_0^2} \,. \tag{20}$$

The above simplified formalism is based on the assumption that the oscillation amplitude δ is sufficiently small in comparison with the length of the cantilever. Obviously, the results derived so far describe only free cantilever oscillations, e. g., oscillations at the absence of any probe-sample interaction. This means d_0 is still so large that no influence of the sample on the probe's oscillation can be detected. If d_0 is now decreased such that a force F affects the motion of the cantilever then a term F/m has to be added to the left-hand side of Eq. (16). In order to consider almost all interactions which could be interesting in force microscopy one has to assume

$$F = F\left(d, \frac{\partial d}{\partial t}\right), \tag{21}$$

which accounts, apart from static interactions, also for dynamic forces. An example for the latter are hydrodynamic effects or eddy-currents (Hoffmann et al., 1997). Since F describes in

the various applications of dynamic-mode force microscopy interactions of various types, i. e., of very different dependence on the probe-sample spacing, the d(t) curves monitored by the deflection sensor and found according to Eq. (16) usually represent enharmonic oscillations. If, however, F(d) can be substituted by a first-order Taylor approximation for $\delta_0 \ll d_0$, then the force microscope detects the compliance or vertical component of the force gradient $\partial F/\partial z$. On the basis of this approximation the cantilever behaves under the influence of the probe-sample interaction as if it would have the modified spring constant

$$c_F = c - \frac{\partial F}{\partial z}, \tag{22}$$

where c is the intrinsic spring constant entering Eq. (5). An attractive probe-sample interaction with $\partial F/\partial z > 0$ will effectively soften the cantilever spring, while a repulsive interaction with $\partial F/\partial z > 0$ will make it effectively stiffer. According to Eq. (6) the change of the apparent spring constant will modify the cantilever's resonant frequency to

$$\omega = \omega_0 \sqrt{1 - \frac{1}{c}\frac{\partial F}{\partial z}}\,. \tag{23}$$

Provided that $\partial F/\partial z \ll c$, the shift in resonant frequency is given by

$$\Delta\omega \approx -\frac{1}{2c}\frac{\partial F}{\partial z}\,. \tag{24}$$

According to Eqs. (19) and (20) a modification of the resonant frequency will result in a change of the probe's oscillation amplitude δ and of the phaseshift α between probe oscillation and driving signal. $\Delta\omega$, δ, and α are experimentally accessible quantities which can be used to map the lateral variation of $\partial F/\partial z$. Phase and amplitude additionally contain information about the damping coefficient γ. Thus, a local variation of this quantity can be separated from the local variation of the compliance by measuring the frequency shift and the change in amplitude or the phase shift. The simple harmonic solution in Eq. (18) evidently shows that the dy-

namic mode of operation can conveniently be based on the employment of lock-in methods. The additional use of certain feedback mechanisms opens different variants of operation.

The most commonly used detection method which is generally referred to as "slope detection" involves driving the cantilever at a fixed frequency ω slightly off resonance. According to Eq. (23) a change in $\partial F/\partial z$ gives rise to a shift in the resonant frequency $\Delta\omega$ and, according to Eq. (19), to a corresponding shift $\Delta\delta$ in the amplitude of the cantilever vibration. $\Delta\delta$ is obviously a maximum at that point of the amplitude-versus-frequency curve where the slope is a maximum. As already discussed in Sect. 3.1 the sensitivity is ultimately determined by thermal noise. A careful analysis (Dürig et al., 1986; McClelland et al., 1987; Martin et al., 1987) shows that the minimum detectable compliance is given by

$$\left(\frac{\partial F}{\partial z}\right)_{\min} = \frac{1}{\delta_{rms}}\sqrt{\frac{2kT\beta}{\omega_0 Q}}\,, \qquad (25)$$

where δ_{rms} is the rms amplitude of the driven cantilever vibration and β is the measurement bandwidth. High Q values can be obtained by the reduction of air damping in vacuum ($< 10^{-3}$ mbar). It might thus appear advantageous to maximize sensitivity by obtaining the highest possible Q. With slope detection, however, increasing the Q restricts the bandwidth of the system. If $\partial F/\partial z$ changes during scanning, the vibration amplitude settles on a new steady-state value after a sufficient length of time given by

$$\tau = \frac{2Q}{\omega_0}\,. \qquad (26)$$

Thus, for a high-Q cantilever in vacuum (Q = 50,000) and a typical resonant frequency of 50 kHz the maximum available bandwidth would be only 0.5 Hz which is unusable for most applications. The dynamic range of the system would be similarly restricted. Because of these restrictions it is not useful to try to increase sensitivity by raising the Q to such high values. Moreover, if the experiments have to be performed in vacuum, e. g., to prevent sample contamination, it may not be possible to obtain low enough Q for an acceptable bandwidth and dynamic range. Therefore, slope detection is unsuitable for most vacuum applications.

An alternative to slope detection is frequency modulation (FM). In the FM detection system a high-Q cantilever vibrating on resonance serves as the frequency-determining component of an oscillator. Changes in $\partial F/\partial z$ cause instantaneous changes in the oscillator frequency which are detected by an FM demodulator. The cantilever is kept oscillating at its resonant frequency utilizing a positive feedback. The vibration amplitude is likewise maintained at a constant level. A variety of methods, including digital frequency counters and phase-locked loops, can be used to measure the oscillator frequency with a very high precision.

In the case of FM detection a careful analysis (Albrecht et al., 1990 b) shows that the minimum detectable force gradient is given by that of Eq. (25) multiplied by $\sqrt{2}$. However, in contrast to slope detection Q and β are absolutely independent in FM detection. Q depends only on the damping of the cantilever and β is set only by the characteristics of the FM demodulator. Therefore the FM detection method allows the sensitivity to be greatly increased by using a very high Q without sacrificing bandwidth or dynamic range.

Contact-mode force microscopy, as discussed so far, relies on the existence of long-range interactions between probe and sample. If no static magnetic and electric fields are involved the only common long-range interactions are in any case van der Waals forces and, in the presence of liquids, capillary forces. Van der Waals forces are weak and carry only limited information on the surface structure. Thus, noncontact-mode force microscopy is on the one hand largely nondestructive but yields on the other hand only a lateral resolution of the order of the probe-sample spacing. In contrast, contact-mode force microscopy has the potential of high spatial resolution. But it also involves the potential for surface perturbation. A way to combine the positive aspects of both modes of operation is given if one oscillates the probe such that there is only an intermittent contact between probe and sample during each oscillation period. This can be realized if the average probe position, i. e., d_0 in Eq. (16), is sufficiently far away from the sample surface. At the same time the driving amplitude δ_0 is chosen sufficiently large to establish the intermittent contact. As a consequence, the small-amplitude approximation in Eq. (22) is no longer valid and the tip experiences the full variation of the probe-sample interaction potential shown in Fig. 8. The intermittent-contact mode, which is generally considered as a special variant of the dynamic modes, does thus obviously not probe a simple force gradient. However, the repulsive forces during intermittent contact lower the

rms oscillation amplitude which yields a highly surface-sensitive signal that can be used for feedback support.

The important point is that the energy transferred from the oscillating probe to the sample surface is in the intermittent-contact mode very much lower than that in the standard contact-mode of operation. This makes the technique especially interesting for the analysis of delicate soft-matter samples (Fig. 14).

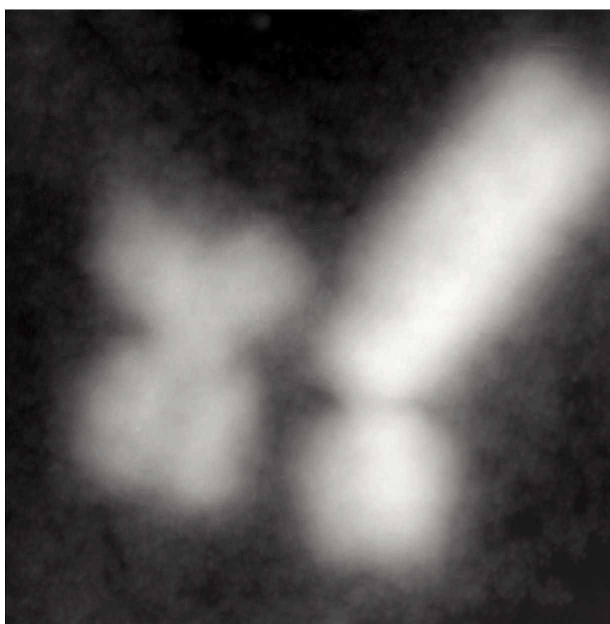

Fig. 14: *Human chromosomes deposited on a glass substrate and imaged by intermittent-contact force microscopy. The image is 3 µm x 3 µm.*

The "intensity" of the intermittent contact can be controlled by appropriately setting the free-vibration amplitude as well as the drop in the amplitude which is kept constant during scanning. Under ambient conditions, amplitudes as large as 10 - 100 nm are frequently used for cantilevers with resonant frequencies of 100 kHz or more. Under liquid immersion the amplitude and its drop can be set much smaller.

Since in all dynamic modes of operation the dynamic properties of the probes are essential, it might be important to search for alternatives with respect to the standard cantilevers as shown in Fig. 2. Especially high resonant frequencies and high quality factors are of interest. One such alternative are quartz oscillators. A well-known oscillator type is the tuning fork, commonly used in, e. g., watches. Using such an element, it is possible to image the surface topog-

raphy of conducting as well as nonconducting samples (Güthner et al., 1989; 1990). The oscillator is driven at its resonant frequency upon approaching the sample surface. Frequency and amplitude significantly change for probe-sample separations below typically 100 µm. The damping strongly depends on the environmental gas pressure which leads to the conclusion that mainly hydrodynamic forces are relevant.

The noncontacting force microscope utilizing quartz oscillators can be considered as a *near-field acoustic microscope*. For a 32 kHz oscillator the wavelength in ambient air is about 1 cm. Since the probe-sample spacing is much smaller, the interaction with the sample takes place in the acoustic near-field regime. The obtained spatial resolution is thus clearly not limited by the acoustic wavelength and the microscope fulfills the requirements for high-resolution near-field microscopy discussed in Sect. 2. Recently the use of quartz rods with high resonant frequency and quality factor has drawn much attention to the possibility of performing Scanning Near-Field Acoustic Microscopy (SNAM) at very high if not atomic resolution. This requires a minimum probe-sample spacing obtained by the intermittent-contact operation or in a real contact mode (see also Sect. 3.8).

A considerable technical advantage in using quartz oscillators is that no relative positioning of oscillator and deflection sensor is needed. The oscillator directly provides information about the local probe-sample interaction in terms of electrical signals. It is thus of increasing importance to employ such oscillators under UHV and low-temperature conditions where the implementation of conventional deflection sensors is often difficult. The usefulness of quartz or piezoelectric oscillators as elements permitting a precise distance control in various scanning probe applications should be emphasized.

One of the hottest topics in the field of microscopy at the present time is the achievement of atomic-scale lateral resolution by noncontact force microscopy. High-resolution information can, of course, be only obtained if the probe-sample spacing is decreased to a tunneling distance. If it is possible to stabilize the cantilever oscillation with a relatively small amplitude, such that there is only intermittently a sufficient approach between probe and sample, the oscillation signal monitored by the deflection sensor contains some information about this intermittent contact. The long-range interactions doe, however, still govern the whole oscillation. The FM approach described above is an appropriate way to perform the experiments

which generally have to take place in UHV. If the cantilever is somehow electrically conducting the intermittent-contact measurements can be combined with intermittent-tunneling microscopy, thus providing simultaneously information on forces and electronic surface properties. Feedback operation can then be supported by the force measurement, by the tunneling current, or by a combination of both. A number of striking experiments (Giessibl, 1995; Shin-ichi Kitamura and Iwatsuki, 1995; Güthner, 1996; Lüthi et al., 1996) has confirmed that the 7x7 surface reconstruction of the Si(111) surface can indeed be imaged with true atomic resolution (Fig. 15).

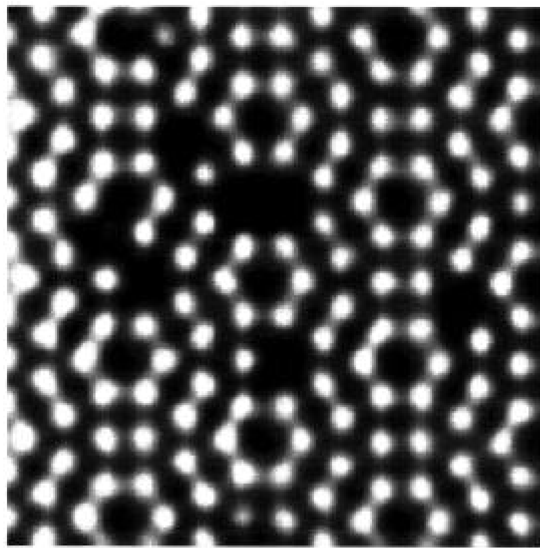

Fig. 15: *Atomic resolution on Si(111) 7 x 7 in noncontact-mode AFM. The grey scale corresponds to variations of the cantilever's oscillation frequency (courtesy by P. Güthner, Omicron Vakuumphysik).*

Other approaches showed (Ueyama et al., 1995) that noncontact-mode AFM also has the potential to image III-V compound semiconductors with atomic resolution. Additional experiments performed very recently involve ionic crystals and even metals. It does not have to be emphasized that the capability of investigating a large variety of sample surfaces with atomic resolution independently of the conductivity of the sample or in combination with tunneling microscopy is a big breakthrough in surface analysis.

3.7 Shear-Force Microscopy

The appearance of shear forces requires that two surfaces are moved laterally with respect to each other. The utilization of shear interactions opens a new possibility in noncontact force microscopy. If a tip with a suitable resonant frequency and quality factor is oscillated not vertically but largely parallel to the sample surface a decrease in the oscillation amplitude can be observed upon probe-sample approach. Originally, shear-force detection was introduced as a mechanism to control and keep constant the probe-sample separation in near-field optical microscopy (Betzig et al., 1992; Toledo-Crow et al., 1992; Grober et al., 1994). In this application the probing tip is the end of a glass fiber which is resonantly dithered using a piezo actuator. The detection of the shear force as a function of lateral position provides, apart from the feedback purposes, a surprisingly accurate image of the sample surface with nanometer resolution. The glass fiber can be substituted by any other suitable probe. Figure 16 shows a comparison between a standard contact-mode AFM image taken on an ordinary CD and a noncontact shear-force image obtained on the same sample. It is obvious that the spatial variation of the shear force clearly represents the surface topography.

The lateral oscillation of the probe and its dependence on probe-sample interactions is fully characterized by the mathematical framework discussed in Sect. 3.6 for a vertical probe oscillation. The axis along which the oscillation takes place has simply to be rotated by 90°. This means in particular that F from Eq. (21) acts along the sample surface and not perpendicular to it. Assuming a permanent or an intermittent probe-sample contact, a decrease of the probe's oscillation amplitude would result from partial sticking or friction in combination with a certain bending of the probe. This mode of operation could somehow be compared with friction-force microscopy or intermittent-contact force microscopy as described above. A mechanical contact of small contact radius between probe and sample can even account for the pronounced dependence of the shear force on the probe-sample spacing which has been observed in vacuum and liquid helium (Gregor et al., 1996). In changing the probe-sample distance the loading force is changed, which has a direct influence on the measured oscillation amplitude.

It is very likely that, apart from direct probe-sample contact, there are additional phenomena leading to measurable shear forces. Especially under ambient conditions interactions may be due to viscous drag across the sample between probe and sample surface contaminant (Moyer

and Paesler, 1993). With this in mind, the force in Eq. (21) definitely becomes dependent on the probe velocity. More precisely, it becomes proportional to the velocity since small velocities have negligible higher-order dependencies. Furthermore, since the forces are frictional the decrease in oscillation amplitude is due to an increase in the damping term in Eq. (19) rather than due to a variation in the resonant frequency. The measured forces are then essentially dissipative but they depend on conservative probe-sample interactions.

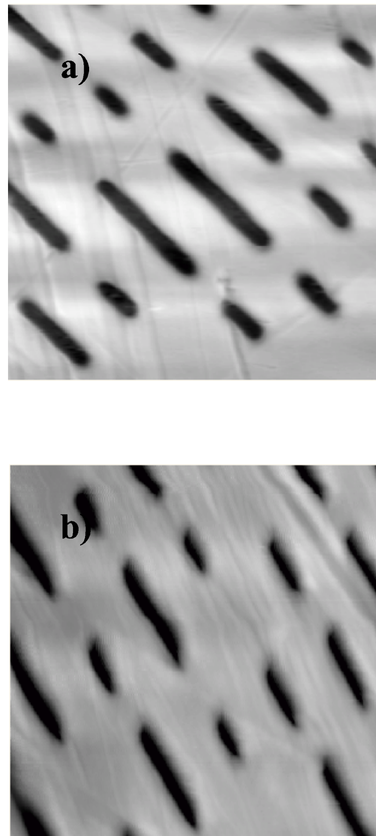

Fig. 16: *The information carrying pits of a compact disc. (a) was taken in the standard contact mode of operation while (b) represents a shear-force image. The scanned area is 10 µm x 10 µm.*

The investigations performed so far show that shear-force detection is a convenient method to control the working distance in SPM. Shear-force microscopy yields information about the surface topography from the nanometer up to the micrometer range, which is qualitatively comparable with the result of standard contact- or noncontact-mode data. However, the actual nature of the shear force is still subject of considerable controversy. Apart from the discussed mechanisms further sources of probe-sample interaction dealt with in Sect. 3.3 may also con-

tribute to the interaction. In any case, shear-force data involves the potential for misinterpretation (Durkan and Shvets, 1996) as any other mode of operation does as well.

3.8 Force Curves and Spectroscopy

Force microscopy is not only capable of providing information about the lateral variation of probe-sample interactions across a sample surface. One can also systematically determine the dependence of the interaction on the probe-sample distance, i. e., the range of the interaction at a given location with respect to the sample surface. Such an investigation is essential in the analysis of the very nature of an unknown interaction. Often the variation of the force looks as in the schematical diagram in Fig. 8. It can, however, also look quite different, as discussed in Sect. 3.3. The basic question is now, how the cantilever's response to a given force variation is.

In tracing a force curve the vertical position of the probe with respect to the sample surface is systematically varied. According to Eq. (5) the acting force leads to a bending Δz of the cantilever. The real probe-sample distance is then given by

$$d = \Delta z - z \,, \tag{27}$$

where bending of the cantilever towards the sample due to an attractive interaction yields a negative Δz value. The probe-sample approach is described by a decreasing magnitude of $z < 0$. What is experimentally recorded are $\Delta z(z)$ plots. Since there is no possibility to independently measure the distance between the outermost atoms of probe and sample, it is difficult to determine the origin of the $F(d)$ diagram in Fig. 8. According to Eq. (27) the probe-sample distance vanishes for $\Delta z = z$, which does, however, not imply $F(d = 0) = 0$. The net force F vanishes if attractive and repulsive forces just balance each other. Then one finds $\Delta z = 0$, which in turn does generally not imply $d = 0$.

The most important experimental finding is, that a force curve like that shown in Fig. 8 cannot be traced reversibly as shown in Fig. 17 (a). Upon probe-sample approach attractive forces lead to a bending of the cantilever towards the sample. This causes a nonlinear $d(z)$ variation

in Eq. (27). If the vertical component of the force gradient, $\partial F/\partial z$, at a sufficiently small probe-sample spacing d exceeds the cantilever's spring constant c, the instability discussed already in Sect. 3.1 causes a jump of the probe to contact. A local minimum in the force curve indicates maximum attraction. Further decrease of the probe-sample spacing increases the loading force and the contact radius. Bending of the cantilever is succesively decreased and vanishes when the repulsive forces balance the attractive ones. Further pushing the probe towards the sample causes the cantilever to bend away from the sample. In the absence of elastic deformation of probe and sample, $d = 0$ in Eq. (27) yields a slope of the $\Delta z(z)$ curve equal to unity. The F(d) curve accordingly exhibits an infinite slope because d remains zero independently of the varying z value.

Upon withdrawing the probe, the motion of the cantilever is reversed. The net loading force continuously decreases. After reversibly reaching the origin of the force curve, which corresponds to the origin of the $\Delta z(z)$ curve, bending of the cantilever is again towards the sample surface. In further trying to separate probe and sample, one finds that they adhere to each other. This phenomenon causes an extended motion of the cantilever with $\Delta z = z$. At a certain point of retraction the net force gradient again becomes equal to the cantilever's spring constant and a jump out of contact occurs. From then on the probe does not experience any interaction with the sample and the cantilever is in its equilibrium position.

Some very important aspects can be concluded from the above comparison between the idealized curve in Fig. 8 and the experimental one in Fig. 17 (a). Most important is the fact that the full F(d) curve is generally not experimentally accessible (Meyer et al., 1988). For $\partial F/\partial d = c$, with d determined by Eq. (23) a cantilever instability occurs. Upon probe-sample approach this instability suddenly decreases d by the instantaneous jump of Δz for a certain z value. The actual Δz value now yields the maximum attractive force F_{att} which is obtained for $z = \Delta z < 0$. From now on, one can reversibly trace a regime with $z = \Delta z$ and $d = 0$ up to repulsive forces, where notable elastic deformation sets on. If there would be no adhesion between probe and sample at all, the probe would jump out of contact if Δz again becomes smaller than F_{att}/c. In any case a certain regime of the F(d) curve which is determined by the distance interval over which the jump takes place is experimentally not accessible. It is obvious that the questionable interval can be decreased by taking sufficiently stiff cantilevers.

Another important aspect is that elastic surface deformations change the slope in the linear regime of $\Delta z(z)$. Since in this case $z > 0$, one obtains $d < 0$ and information about the involved elasticity is additionally provided by the F(d) curve. For negative values of d the probe penetrates the sample surface and the slope of the F(d) curve turns to a finite value. Inelastic surface deformation leads to irreversibilities and eventually to characteristic jumps in the $\Delta z(z)$ curve (Landman et al., 1990). Under such circumstances the force microscope can be operated as "nanoindentor" with some advantages in comparison to conventional indentation hardness testers (Pethica et al., 1983).

Even if no inelastic surface deformation is involved, force curves generally exhibit considerable hysteresis as in Fig. 17 (a). This hysteresis is due to an adhesive force between probe and sample. For clean surfaces of probe and sample adhesion can result from covalent or metallic binding between probe and sample atoms (Landman et al., 1990). The pronounced hysteresis, however, which is usually observed under ambient conditions is due to capillary forces (Hartmann, 1994). These often initiate already the jump to contact upon approaching the probe to the sample. If the probe is then retracted the liquid meniscus deforms with increasing substrate-probe separation. Sometimes it can be elongated to a length of more than 100 nm. Upon reaching the maximum adhesive force F_{adh}, the capillary breaks and the cantilever jumps back to its equilibrium position. Usually, the magnitude of F_{adh} is much larger than that of F_{att} which causes a huge hysteresis. In contrast, F_{adh} should be reduced to the real substrate-probe adhesion if the force curve is taken in a liquid (Weisenhorn et al., 1989). Indeed, as can be seen in Fig. 17 (b) the hysteresis is much reduced under liquid immersion.

Alternatively to the F(d) curve, also the $\partial F/\partial z(d)$ curve can be taken. The probe is then operated in the dynamic mode as desribed in Sect. 3.6. The quantity derived from the cantilever oscillation is, however, only equal to the numerically calculated derivative of the F(d) curve if no hydrodynamic or other dissipative interactions are involved. In tracing the range of the probe-sample interaction, the interaction is systematically varied with respect to magnitude and sign. This is often called "force spectroscopy". As in other spectroscopies, however, it is not always of importance to vary the energy over the whole accessible range. Sometimes it is more interesting to map local variations of a given characteristic feature whithin the whole spectrum. With respect to the force curves discussed above, characteristic quantities are F_{att}, F_{adh}, and the surface elasticity c_s.

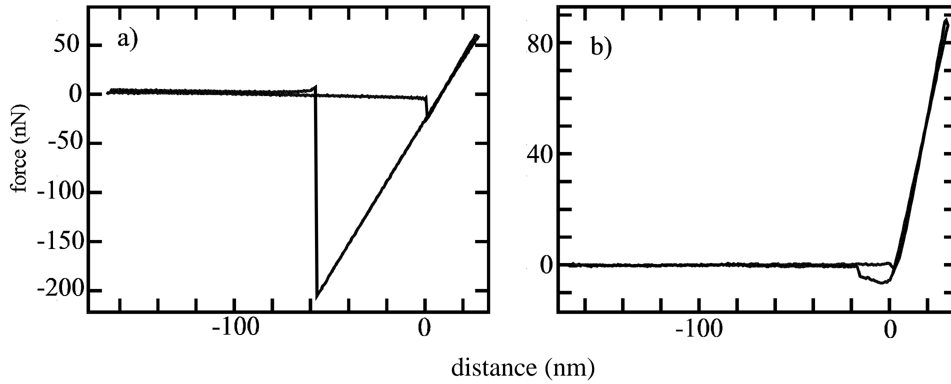

Fig. 17: *Force curves taken on a hydrophilic Si(100) substrate using an Si cantilever. (a) was taken in ambient air, while (b) was taken under complete immersion of probe and sample in water.*

Spatial adhesion maps represent the lateral variation of F_{adh} due to material inhomogeneities and the surface topography (Mizes et al., 1991). If F_{adh} is dominated by capillary interactions, the nanoscale behavior of liquid thin films, in particular that of polymers, can be studied in detail (Mate et al., 1989). This provides qualitatively new information on surface forces of molecular film arrangements (Burnham et al., 1990; Blackman et al., 1990). In the same way as F_{adh} also F_{att} can be mapped.

The surface elasticity is roughly characterized by an effective spring constant c_s. If a sample exhibits a finite c_s, a sufficient loading force makes the probe penetrate the sample. This process is described by Eq. (27) for a negative probe-sample spacing d. For a given loading force F the cantilever deflection Δz then depends on the local value of c_s and, of course, on the probe's spring constant c:

$$\Delta z = -\frac{c_s}{c} d \; . \tag{28}$$

With Eq. (27) one obtains

$$c_s = \frac{\Delta z}{z - \Delta z} c \tag{29}$$

in terms of the experimentally accessible quantities. This result tells us in particular that the cantilever's spring constant has to be chosen appropriately. Experimentally, elasticity maps are obtained in a dynamic contact or intermittent-contact mode by modulating z (Maivald et al., 1991). This causes a corresponding oscillation of Δz from which the surface elasticity c_s can be derived according to Eq. (29).

4. Nanometer-Scale Modification of Surfaces

An image acquired by a scanning force microscope is a collection of data representing the result of the particular experiment performed at any addressed location of the raster-scanned area.

This point of view which applies to any SPM investigation has already been discussed in detail in Sect. 2. In the ideal case the probe-sample interactions involved in any kind of microscopy are weak enough to not permanently modify nor the probe neither the sample. On the other hand, any interaction involves forces. If these forces do not permanently or temporarily affect the sample, there must be a restoring force which allows the sample to recover after taking away the probe, or which even allows the sample to balance the interaction in the presence of the probe. A big advantage of the scanning force microscope is that the probe-sample interaction, e. g., the loading force exerted by the probe on the sample, can be varied over a considerable range. This range generally includes a regime where the chosen strength of interaction exceeds a critical value leading to more or less durable sample modifications. In the present context such a modification is considered as a generated nanostructure if it is at least stable enough to survive after removing the probe from the respective location. Usually the modification should be at least stable enough to be imaged by the same probe with which it was generated. *A priori*, surface manipulations thus involve metastable as well thermodynamic equilibrium configurations of the sample. Nanomodifications at sample surfaces can be produced by utilizing several of the interactions discussed in Sect. 3.3. Sufficiently strong interactions between probe and sample can be generated in the contact- as well as in the non-contact-mode operation.

Nanotechnology deals with individual objects, the lateral dimensions of which are in the range of 0.1 nm to 100 nm. For such small objects the physical properties are strongly influenced by size and surface effects because the geometrical dimensions approach characteristic lengths associated with elementary processes. Examples for such lengths are the electron mean path, the de Broglie wavelength, the coherence lengths in a superconductor, or the ferromagnetic exchange length. Nanotechnology is considered as a key technology strongly influencing future technical developments, in particular in the field of information technology. The well-defined production of nanometer-scale structures involves basic research on nanopositioning and nanocontrol approaches, on nanoprecision machining, on the possibilities of utilizing self-assemblence and autoreproduction phenomena, and on possibilities to link nanostructures to conventional microstructures. Most important is, however, a profound understanding of all relevant physical properties of matter at the nanometer scale and the resulting properties of nanodevices. In this task SFM, and SPM in general, is a very valuable tool for the fabrication as well as for the analysis of nanoscale structures.

A straightforward method to modify the surface of a sample is to operate the force microscope in the contact or intermittent-contact mode with sufficiently high loading forces (Fig. 18).

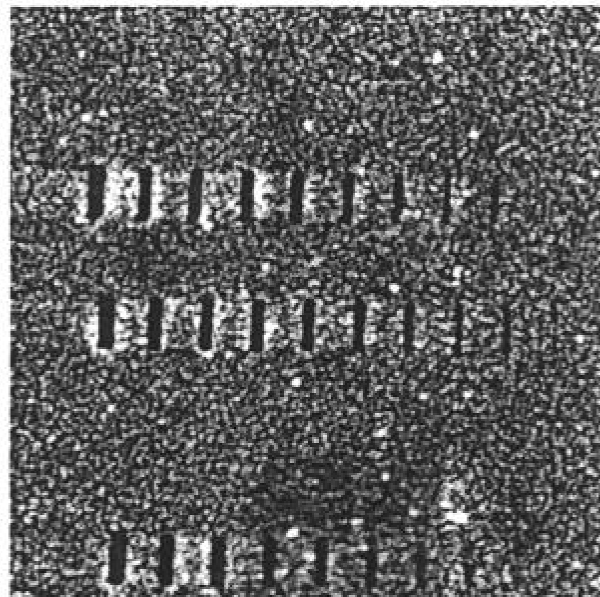

Fig. 18: *Nanomodifications in an Au thin film, performed by AFM in an intermittent-contact mode. The structures were imaged with the same probe with which they were produced. The scanned area is 3.2 µm x 3.2 µm. The smallest structures are about 100 nm in width.*

Modifications can be performed on conducting, semiconducting and insulating samples. On appropriate substrates and upon carefully choosing the operational parameters, structures with dimensions below 10 nm can be reproducibly generated (Albrecht, 1989; Jung et al., 1992). AFM-induced mechanical surface manipulations with a sufficient stability can be used either to produce complete thin film devices or in a proper combination with microfabrication techniques to optimize particular components of a given microstructure (Fig. 19).

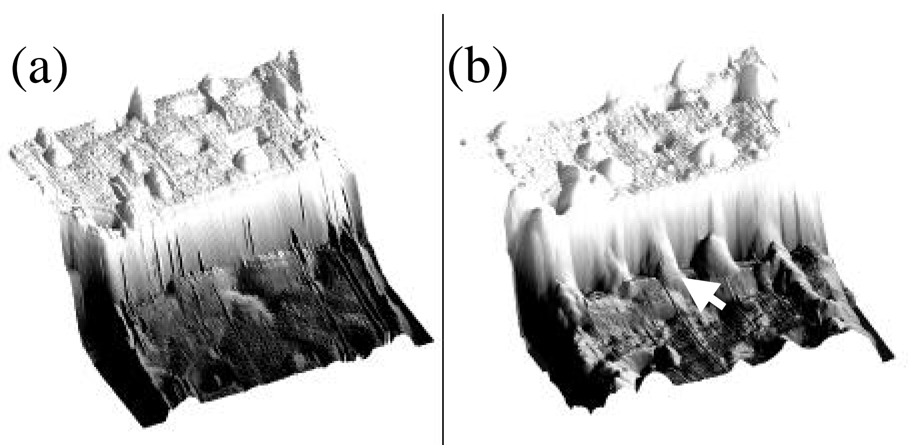

Fig. 19: *Step-etch Josephson junction in a high-T_c superconducting thin film. (a) shows the original junction, while (b) shows the junction after mechanical modification by AFM. The arrow indicates one out of five clearly visible "nanobridges" which have been deposited at the step. The procedure can be used to tune and optimize the junctions of a SQUID. The scan range is 5 µm x 5 µm. (Drechsler et al., 1997).*

Apart from a direct surface structuring also the usefulness of nanostructured masks in combination with conventional etching techniques has been demonstrated. In the noncontact mode of operation sufficiently strong probe-sample interactions are obtained by utilizing long-range electromagnetic, electrostatic, and magnetostatic fields. This offers a variety of possibilities to modify and functionalize surfaces with high resolution. It has, e. g., been shown that a considerable amplification of the electromagnetic field can locally result if a probing tip is illuminated by a laser beam (Jersch and Dickmann, 1996). Using this phenomenon, the sample surface can be modified by a local thermal treatment. It has further been demonstrated that by applying voltage pulses to the tip patterns of trapped charge can be written into insulating thin films with a very high resolution (Barrett and Quate, 1991). Using ferromagnetic probes with

a sufficiently high magnetic stray field the magnetization of a ferromagnetic sample can be locally reversed (Fig. 20). Thus, it is even possible to write well-defined magnetic patterns into pretty hard magnetic materials (Moreland and Rice, 1990; Göddenhenrich et al., 1992).

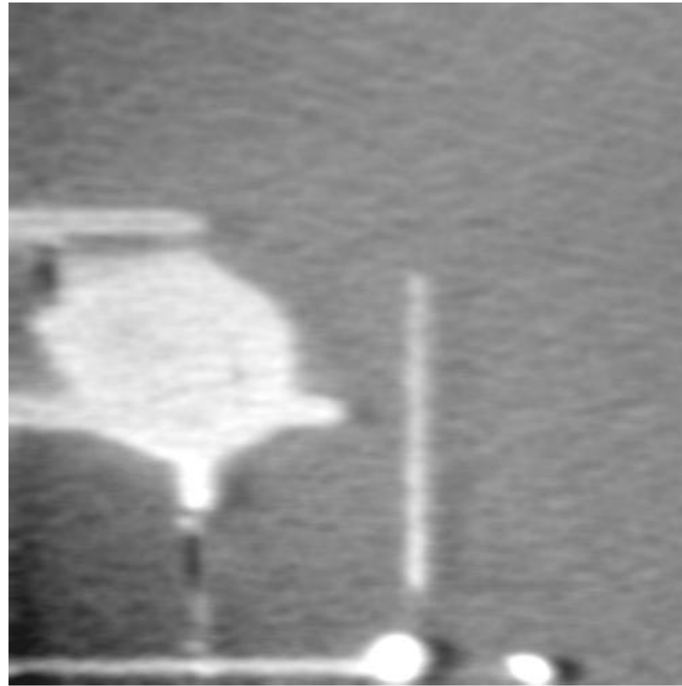

Fig. 20: *Magnetic domains in a 10 nm thick Fe film. The domains were generated by approaching a ferromagnetic probe to the thin film. In thermodynamic equilibrium the easy axis of magnetization lies in the sample surface. The stray field of the magnetic probe locally produces a metastable state where the magnetization is directed along the surface normal in either direction (black and white domains). After lifting the probe to a certain minimum probe-sample separation, the magnetic configuration can be imaged without any destructive influence. The imaged area is 18 μm x 18 μm.*

At the present time the various approaches to manipulate surfaces at a nanometer scale can be considered as basic research yielding the basis for future directions in nanotechnology. SPM makes nanolithography accessible to almost everybody because big and expensive facilities, as known from electron-beam or x-ray lithographies are no more necessarily required to produce small structures for basic investigations. The industrial production of nanoscale devices, however, requires batch fabrication approaches, i. e., the parallel processing of large areas. The latter task cannot yet be solved by AFM-based approaches. This may, however, change in

future. First steps towards the microfabrication of multiple sensor tips and whole SPM instruments were already presented (Busta et al., 1989; Akamine et al., 1989; Albrecht, 1989; Albrecht et al., 1990 c; Tsukamoto et al., 1991).

5. Conclusions and Outlook

AFM is presently the most widely used variant in the field of SPM. Within ten years the technique has become an extremely powerful tool in surface analysis. It has been discussed in detail that possible investigations are not restricted to contact-mode surface profilometry but that intermittent-contact and noncontact modes of operation open the possibility to measure manifold interactions between a local probe and the sample surface. It is thus more adequate to denote the whole family of possible variants by the acronym SFM, emphasizing that one is dealing with various scanning force methods. One of these methods is AFM which is capable of achieving even an atomic resolution. Contact-mode operation also involves LFM which maps frictional forces at an atomic or nanometer scale. A link between contact-mode operation and real noncontact-mode operation is intermittent-contact force microscopy. This variant is partucularly useful in imaging delicate soft-matter samples at very high resolution. Noncontact force microscopy opens the possibility to detect long range interactions such as van der Waals forces, electrostatic forces, and magnetostatic forces. Detailed information about the nature and range of an unknown interaction can be obtained from force-versus-distance curves. Upon suitable operation these curves also involve information about surface elasticity and adhesion forces.

Force microscopes can be operated in static as well as in dynamic modes, utilizing all relevant mechanical properties which the microfabricated probes offer. In state-of-the-art instruments the sensitivity is limited only by the thermal excitation noise of the probes. It is thus interesting to operate force microscopes under low-temperature conditions and considerable effort is presently put into the development of respective instruments. Additionally, force microscopes can be operated in a gas atmosphere, in UHV, or under liquid immersion.

Apart from largely nondestructive probing, force microscopes can also be employed as instruments which are suitable to modify and functionalize sample surfaces at a nanometer

scale. For this application a big advantage is that nanomanipulation and subsequent imaging can be performed with the same instrument by solely changing appropriate parameters of operation. Nanolithography thus becomes accessible to everybody who employs force microscopy. This aspect provides an optimum basis for developing new approaches in nanotechnology in many laboratories.

Future effort in force microscopy will be concentrated on both further improving the instrument and employing the technique for more and more applications in basic as well as applied research. Further technical developments will predominantly involve the application of force microscopy in UHV, under high magnetic fields, and at a variable sample temperature. These developments are strongly related to the development of improved cantilever-deflection sensors avoiding complicated mechanical adjustments. Microfabrication and the batch production of arrays of force probes are essential to further push some approaches being considered as very promising in nanotechnology. Applications being already established in basic research will become as well established in industrial production processes, e. g., for purposes of quality control. New applications will again first be introduced in basic research. These will involve the utilization of particular probe-sample interactions which have so far not been used for high-resolution imaging. An example for the latter is spin resonance force microscopy (Rugar et al., 1992). Force microscopes will gain considerable importance especially in soft-matter science. The analysis of individual intermolecular interactions will open completely new possibilities in biology and biochemistry. In this field it will be of predominant importance to systematically functionalize probes with specific molecular structures and to operate the force microscope at highest sensitivity in physiological environments.

Acknowledgment

The author would like to thank all members of his research group who provided him with high-quality viewgraphs. In particular U. Memmert, A.Drechsler, and R. Houbertz contributed much in collecting experimental data. Mrs. S. Neumann exhibited much patience in carefully processing the typescript.

References

Abraham, D. W., Williams, C. C., Shinkman, J., and Wickramasinghe, H. K. (1991) J. Vac. Sci. Technol. B **9**, 703.

Abraham, F. F., and Batra, I. P. (1989) Surf. Sci. **209**, L125.

Akamine, S., Albrecht, T. R., Zdeblick, M. J., and Quate, C. F. (1989) IEEE Electron Device Lett. **10**, 490.

Albrecht, T. R., (1989) Ph. D. Thesis, Stanford University.

Albrecht, T. R., Akamine, S., Carver, T. E., and Quate, C. F. (1990 c) J. Vac. Sci. Technol. A **8**, 3386.

Albrecht, T. R., Akamine, S., Zdeblick, M. J., and Quate, C. F. (1990 a) J. Vac. Sci. Technol. A **8**, 317.

Albrecht, T. R., Grütter, P., Horne, D., and Rugar, D. (1990 b) IBM Research Report RJ 7681.

Alexander, S., Hellemans, L., Marti, O., Schneir, J., Elings, V., Hansma, P. K., Longmire, M., and Gurley, J. (1989) Appl. Phys. Lett. **65**, 164.

Amelincks, S., van Dyck, D., van Landuyt, J., and van Tendeloo, G., Eds. (1997) *Handbook of Microscopy* (VCH, Weinheim): General Introduction.

Anders, M., Thaer, M., and Heiden, C. (1987) Surf. Sci. **181**, 176.

Bai, Ch. (1995) *Scanning Tunneling Microscopy and its Application* (Springer, Berlin).

Barrett, R. C., and Quate, C. F. (1991) J. Appl. Phys. **70**, 2725.

Baumeister, T., and Marks, L.S. (1967) *Standard Handbook for Mechanical Engineers* (McGraw-Hill, New York.)

Besocke, K. (1987) Surf. Sci. **181**, 139.

Betzig, E., Finn, P. L., and Weiner, J. S. (1992) Appl. Phys. Lett. **60**, 2484.

Binnig, G. (1992) Ultramicroscopy **42-44**, 7.

Binnig, G., and Rohrer, H. (1982) Helv. Phys. Acta **55**, 726.

Binnig, G., and Smith, D. P. E. (1986) Rev. Sci. Instrum. **57**, 1988.

Binnig, G., Quate, C. F., and Gerber, Ch. (1986) Phys. Rev. Lett. **56**, 930.

Binnig, G., Rohrer, H., Gerber, Ch., and Weibel, E. (1982) Phys. Rev. Lett. **49**, 57; Appl. Phys. Lett. **40**, 178; Physica B **109/110**, 2075.

Blackman, G. S., Mate, C., M., and Philpott, M. R. (1990) Phys. Rev. Lett. **65**, 2270.

Bonnell, D. A., Ed. (1992) *Scanning Tunneling Microscopy: Theory, Techniques and Applications* (VCH Press, New York).

Burnham, N. A., Dominguez, D. D., Mowery, R. L., and Colton, R. J. (1990) Phys. Rev. Lett. **64**, 1931.

Busta, H. H., Shadduck, R. R., and Orvis, W. J. (1989) IEEE Trans. Electron Devices **36**, 2679.

Chen, C. J. (1992) Appl. Phys. Lett. **60**, 132.

Chen, C. J. (1993) *Introduction to Scanning Tunneling Microscopy* (Oxford Unversity Press, New York).

Ciraci, S., Baratoff, A., and Batra, I. P. (1990) Phys. Rev. B **41**, 2763.

Coombs, J. H., and Pethica, J. B. (1986) IBM J. Res. Develop. **30**, 443.

Corb, B. W., Ringger, M., and Güntherodt, H.-J. (1985) J. Appl. Phys. **58**, 3947.

Deb, B. M. (1973) Rev. Mod. Phys. **45**, 22.

Demuth, J. E., Hamers, R. J., Tromp, R. M., and Welland, M. E. (1986) J. Vac. Sci. Technol. A **4**, 1320; IBM J. Res. Develop. **30**, 396.

den Boef, A. J. (1989) Appl. Phys. Lett. **55**, 439.

den Boef, A. J. (1991) Rev. Sci. Instrum. **62**, 88.

Drechsler, A., Pitzius, P., and Hartmann, U. (1997) to be published.

Ducker, W. A., Cook, R. F., and Clarke, D. R. (1990) J. Appl. Phys. **67**, 4045.

Dürig, U., Gimzewski, J. K., Pohl, D. W., and Schlitter, R. (1986) IBM Research Report RZ 15

Durkan, C., and Shvets, I. (1996) J. Appl. Phys. **79**,1219.

Dworak, V., Pitzius, P., and Hartmann, U. (1997) to be published.

Erlandsson, R., Hadziioannou, G., Mate, C. M., McClelland, G. M., and Chiang, S. (1988 b) J. Chem. Phys. **89**, 5190.

Erlandsson, R., McClelland, G. M., Mate, C. M., and Chiang, S. (1988 a) J. Vac. Sci. Technol. A **6**, 266.

Euler, R., Memmert, U., and Hartmann, U. (1997) Rev. Sci. Instrum. **68**, 1776.

Fein, A. P., Kirtley, J. R., and Feenstra, R. M. (1987) Rev. Sci. Instrum. **58**, 1806.

Frohn, J., Wolf, J. E., Besocke, K., and Teske, M. (1989) Rev. Sci. Instrum. **60**, 1200.

Gewirth, A. A., and Siegenthaler, H., Eds. (1995) *Nanoscale Properties of the Solid/Liquid Interface* (Kluwer, Dodrecht) Nato ASI Series E, Vol. 288.

Giessibl, F. J. (1995) Science **267**, 68.

Göddenhenrich, Th., Hartmann, U., and Heiden, C. (1988) J. Microsc. **152**, 527.

Göddenhenrich, Th., Hartmann, U., and Heiden, C. (1992) Ultramicroscopy **42-44**, 256.

Göddenhenrich, Th., Lemke, H., Hartmann, U., and Heiden, C. (1990 a) J. Vac. Sci. Technol. A **8**, 383.

Göddenhenrich, Th., Lemke, H., Mück, M., Hartmann, U., and Heiden, C. (1990 b) Appl. Phys. Lett. **57**, 2612.

Gould, S. A. C., Burke, K., and Hansma, P. K. (1989) Phys. Rev. B **40**, 5363.

Gregor, U. J., Blome, P. G., Schöfer, J., and Ulbrich, R. G. (1996) Appl. Phys. Lett. **63**, 307.

Grober, R. D., Harris, T. D., Trautman, J. K., Betzig, E., Wegscheider, W., Pfeiffer, L., and West, K. (1994) Appl. Phys. Lett. **64**, 1421.

Güntherodt, H.-J., Anselmetti, D., and Meyer, E., Eds. (1995) Forces in Scanning Probe Methods (Kluwer, Dodrecht) Nato ASI Series E, vol. 286.

Güthner, P. (1996) J. Vac. Sci. Technol. B **14**, 2428.

Güthner, P., Fischer, U., and Dransfeld, K. (1989) Appl. Phys. B **48**, 89.

Güthner, P., Schreck, E., Dransfeld, K., and Fischer, U. (1990) in: *Scanning Tunneling Microscopy,* Behm, R. J., Garcia, N., and Rohrer, H., Eds., (Kluwer, Dodrecht) p. 507.

Hartmann, U. (1988) J. Appl. Phys. **64**, 1561.

Hartmann, U. (1990/91), Phys. Rev. B **42**, 1541; Phys. Rev. B **43**, 2404.

Hartmann, U. (1994) Advances in Electronics and Electron Physics **87**, 49.

Hartmann, U., Göddenhenrich, T., and Heiden, C. (1991) J. Magn. Magn. Mat. **101**, 263.

Heer, C. V. (1972) *Statistical Mechanics, Kinetic, Theory, and Stochastic Processes* (Academic Press, New York).

Hoffmann, B., Houbertz, R., and Hartmann, U. (1997) European Workshop on Microtechnology and Scanning Probe Microscopy, Mainz, Germany: Extended abstract.

Israelachvili, J. N. (1985) *Intermolecular and Surface Forces* (Academic Press, London).

Itoh, T., and Suga, T. (1993) Techn. Dig. Int. Conf. Solid State Sensors and Actuators (Transducer's 93, Yokohama) p. 610.

Jersch, J., and Dickmann, K. (1996) Appl. Phys. Lett. **68**,868.

Jung, T. A., Moser, A., Hug, H. J., Brodbeck, D., Hofer, R., Hidler, H. R., and Schwarz, U. D. (1992) Ultramicroscopy **42-44**, 1446.

Kaiser, W. J., and Jaklevic, R. C. (1988) Rev. Sci. Instrum. **59**, 537.

Landman, U., Luedtke, W. D., and Nitzan, A. (1989 a) Surf. Sci. **210**, L177.

Landman, U., Luedtke, W. D., and Ribarsky, M. W. (1989 b) J. Vac. Sci. Technol. A **7**, 2829.

Landman, U., Luedtke, W. D., Burnham, N. A., and Colton, R. J. (1990) Science **248**, 454.

Leinenbach, P., Memmert, U., Schelten, J., and Hartmann, U. (1997) European Workshop on Microtechnology and Scanning Probe Microscopy, Mainz, Germany: Extended abstract.

Lemke, H., Göddenhenrich, Th., Bochem, H.-P., Hartmann, U., and Heiden, C. (1990) Rev. Sci. Instrum. **61**, 2538.

Lüthi, R., Meyer, E., Bammerlin, M., Baratoff, A., Lehmann, T., Howald, L., Gerber, Ch., and Güntherodt, H.-J. (1996) Z. Phys. B - Condensed Matter **100**, 165.

Lyding, J. W., Skala, S., Hubacek, J. S., Brockenbrough, R., and Gammie, G. (1988) Rev. Sci. Instrum. **59**, 1897.

Maganov, S. N., and Whangbo, M. H. (1996) *Surface Analysis with STM and AFM* (VCH, Weinheim).

Maivald, P., Butt, H. J., Gould, S. A. C., Prater, C. B., Drake, B., Gurley, J. A., Elings, V. B., and Hansma, P. K. (1991) Nanotechnology **2**, 103.

Mamin, H. J., Abraham, D. W., Ganz, E., and Clarke, J. (1985) Rev. Sci. Instrum. **56**, 2168.

Marti, O., and Amrein, M., Eds. (1993) *STM and SFM in Biology* (Academic Press, San Diego).

Martin, Y., Abraham, D. W., and Wickramasinghe, H. K., (1988) Appl. Phys. Lett. **52**, 1103.

Martin, Y., and Wickramasinghe, H. K. (1987) Appl. Phys. Lett. **50**, 1455.

Martin, Y., Williams, C. C., and Wickramasinghe, H. K. (1987) J. Appl. Phys. **61**, 4723.

Mate, C. M., Lorenz, M. R., and Novotny, U. J. (1989) J. Chem. Phys. **90**, 7550.

Mate, C. M., McClelland, G. M., Erlandsson, R., and Chiang, S. (1987) Phys. Rev. Lett. **59**, 1942.

McClelland, G. M. (1989), in: *Adhesion and Friction*, Grunze, M., and Kreuzer, H. J., Eds. (Springer, Berlin) p. 1.

McClelland, G. M., and Cohen, S. R. (1990), in: *Chemistry and Physics of Solid Surfaces VIII*, Vanselow, R., and Howe, R. Eds. (Springer, Berlin) p. 419.

McClelland, G. M., Erlandsson, R., and Chiang, S. (1987) in: *Review of Progress in Qunatitative Non-Destructive Evaluation*, Thompson, D. O., and Chimenti, D. E., Eds. (Plenum, New York) vol. 6, p. 307.

Memmert, U., Hodel, U., and Hartmann, U. (1996) Rev. Sci. Instrum. **67**, 2269.

Meyer, E., Heinzelmann, H., Brodbeck, D., Overnay, G., Overnay, R., Howald, L., Hug, H., Jung, T., Hidber, H.-R., and Güntherodt, H.-J. (1991) J. Vac. Sci. Technol. B **9**, 1329

Meyer, E., Heinzelmann, H., Grütter, P., Jung, Th., Weisskopf, Th., Hidler, H.-R., Lapka, R., Rudin, H., and Güntherodt, H.-J. (1988) J. Microsc. **152**, 269.

Meyer, G., and Amer, N. M. (1988) Appl. Phys. Lett. **53**,1045.

Meyer, G., and Amer, N. M. (1990) Appl. Phys. Lett. **56**, 2100.

Mizes, H. A., Loh, K. G., Miller, R. J. D., Ahuja, S. K., and Grabowski, E. (1991) Appl. Phys. Lett. **59**, 2901.

Moreland, J., and Rice, P. (1990) Appl. Phys. Lett. **57**, 310.

Morita, S., Ishizaka, T., Sugawara, Y., Okada, T., Mashima, S., Imai, S., and Mikoshiba, N. (1989) Jpn. J. Appl. Phys. **28**, L 1634.

Morita, S., Ishizaka, T., Sugawara, Y., Okada, T., Mishima, S., Imai, S., and Mikoshiba, N. (1989) Jpn. J. Appl. Phys. **28**, L 1634.

Moser, A., Hug, H. J., Parashikov, I., Stiefel, B., Fritz, O., Thomas, H., Baratoff, A., and Güntherodt, H.-J. (1995) Phys. Rev. Lett. **74**, 1847.

Moyer, P. J., and Paesler, A., (1993) SPIE Conf. Proc., vol. 1855, p. 58.

Mulhern, P. J., Hubbert, T., Arnold, C. S., Blackford, B. L., and Jericho, M. H. (1991) Rev. Sci. Instrum. **62**, 1280.

Neubauer, G., Cohen, S. R., McClelland, G. M., Horne, D., and Mate, C. M. (1990) Rev. Sci. Instrum. **61**, 2296.

Niedermann, Ph., Emch, R., and Descouts, P. (1988) Rev. Sci. Instrum. **59**, 368.

Pethica, J. B., Hutchings, R., and Oliver, W. C. (1983) Phil. Mag. A **48**, 293.

Pohl, D. W. (1986) IBM J. Res. Develop. **30**, 417.

Pohl, D. W. (1987) Rev. Sci. Instrum. **58**, 54.

Pohl, D. W., Denk, W., and Lanz, M. (1984) Appl. Phys. Lett. **44**, 651.

Ringger, M., Corb, B. W., Hidber, H.-R., Schlögl, R., Wiesendanger, R., Stemmer, A., Rosenthaler, L., Brunner, A. J., Oelhafen, P. C., and Güntherodt, H.-J. (1986) IBM J. Res. Develop. **30**, 500.

Rugar, D. Yannoni, C. S., Sidles, J. A. (1992) Nature **360**, 563.

Rugar, D., and Hansma, P. (1990) Physics Today, October issue, p. 23.

Rugar, D., Mamin, H. J., and Guethner, P. (1989) Appl. Phys. Lett. **55**, 2588.

Rugar, D., Mamin, H. J., Erlandsson, R., Stern, J. E., and Terris, B. D. (1988) Rev. Sci. Instrum. **59**, 2337.

Rugar, D., Mamin, H. J., Güthner, P., Lambert, S. E., Stern, J. E., McFadyen, I., and Yogi, T. (1990) J. Appl. Phys. **68**, 1169.

Sáenz, J. H., Garcia, N., Grütter, P., Meyer, E., Heinzelmann, H., Wiesendanger, R., Rosenthaler, L., Hidber, H. R., and Güntherodt, H.-J. (1987) J. Appl. Phys. **62**, 4293.

Sarid, D. (1991) *Scanning Force Microscopy with Applications to Electric, Magnetic, and Atomic Forces* (Oxford University Press, New York).

Saurenbach, F., and Terris, B. D. (1990), Appl. Phys. Lett. **56**, 1703.

Scheinfein, M. R., Unguris, J., Pierce, D. T., Celotta, R. J. (1990) J. Appl. Phys. **67**, 5932.

Schönenberger, C., and Alvarado, S. F. (1990 a), Phys. Rev. Lett. **65**, 3162.

Schönenberger, C., and Alvarado, S. F. (1990 b) Z. Phys. B **80**, 373.

Shin-ichi Kitamura, and Iwatsuki, M. (1995) Jpn. J. Appl. Phys. **34**, L 145.

Siebel, E., Memmert, U., and Hartmann, U. (1997) to be published.

Smith, D. P. E., and Binnig, G. (1986) Rev. Sci. Instrum. **57**, 2630.

Smith, D. P. E., and Elrod, S. A. (1985) Rev. Sci. Instrum. **56**, 1970.

Stern, J. E., Terris, B. D., Mamin, H. J., and Rugar, D. (1988) Appl. Phys. Lett. **53**, 2717.

Takata, U., Hosoki, S., Hosaka, S. and Tajima, T. (1989) Rev. Sci. Instrum. **60**, 789.

Terris, B. D., Stern, J. E., Rugar, D., and Mamin, H. J. (1989/90) Phys. Rev. Lett. **63**, 2669; J. Vac. Sci. Technol. A **8**, 374.

Toledo-Crow, R., Yang, P. C., Chen, Y., and Vaez-Iravani, M. (1992) Appl. Phys. Lett. **60**, 2957.

Tortonese, M., Yamada, H., Barret, R. C., and Quate, C. F. (1991) Tech. Dig. Int. Conf. Solid State Sensors and Actuators (Transducers 91, San Francisco) p. 448.

Tsukamoto, S., Lin, B., and Nakagiri, N. (1991) Rev. Sci. Instrum. **62**, 1761.

Ueyama, H., Ohta, M., Sugawara, Y., and Morita, S. (1995) Jpn. J. Appl. Phys. **34**, L 1068.

Uozumi, K., Nakamoto, K., and Fujioka, K. (1988) Jpn. J. Appl. Phys. **27,** L 123.

Weisenhorn, A. L., Hansma, P. K., Albrecht, T. R., and Quate, C. F. (1989) Appl. Phys. Lett, **54**, 2651.

Wiesendanger, R. (1994) *Scanning Probe Microscopy and Spectroscopy* (Cambridge University Press, Cambridge).

Wiesendanger, R., and Güntherodt, H.-J., Eds. (1992/93) *Scanning Tunneling Microscopy I-III*, (Springer, Berlin), 2nd eds. 1994-96.

Wiesendanger, R., Anselmetti, D., and Güntherodt, H.-J. (1990 a) Europhys. News **21**, 72.

Wiesendanger, R., Bürgler, D. Tarrach, G., Anselmetti, D., Hidber, H. R., and Güntherodt, H.-J. (1990 b) J. Vac. Sci. Technol. A **8**, 339.

Williamson, J. B. P. (1967/68) Proc. Inst. Mech. Eng., London **182** (3K), 21.

Zhong, W., and Tománek, D. (1990) Phys. Rev. Lett. **64**, 3054.